Scientific Research Publishing

International Journal of Geosciences, 2025, 16(10), 762-793
https://www.scirp.org/journal/ijg
ISSN Online: 2156-8367
ISSN Print: 2156-8359

# Li-Sn and Pb-Zn Type Mineralization in the Birimian Greenstone Belt of Banfora. Recommendations for the Exploration of Strategic and Base Metals, Burkina Faso, West Africa

**Abdoulaye Ouédraogo[1,2*], Kafohé Azise Héma[2], Mamadou Nimi[2], Seta Naba[1], Urbain Wenmenga[1]**

[1]Laboratoire Géosciences et Environnement (LaGE), Département des Sciences de la Terre, Unité de Formation et de Recherche en Sciences de la Vie et de la Terre, Université Joseph KI-ZERBO, Ouagadougou, Burkina Faso
[2]Bureau des Mines et de la Géologie du Burkina (BUMIGEB), Ouagadougou, Burkina Faso
Email: *abdouloued@gmail.com

**How to cite this paper:** Ouédraogo, A., Héma, K.A., Nimi, M., Naba, S. and Wenmenga, U. (2025) Li-Sn and Pb-Zn Type Mineralization in the Birimian Greenstone Belt of Banfora. Recommendations for the Exploration of Strategic and Base Metals, Burkina Faso, West Africa. *International Journal of Geosciences*, **16**, 762-793.
https://doi.org/10.4236/ijg.2025.1610038

**Received:** August 26, 2025
**Accepted:** October 27, 2025
**Published:** October 30, 2025

Copyright © 2025 by author(s) and Scientific Research Publishing Inc.
This work is licensed under the Creative Commons Attribution International License (CC BY 4.0).
http://creativecommons.org/licenses/by/4.0/

Open Access

## Abstract

Regional exploration of base and strategic metals (Li, Nb, Ta, Sn) in the Kangounadéni sector, part of the Banfora Belt (Paleoproterozoic greenstone belt, West African Craton), was conducted using stream sediment and soil sampling around the two-micas leucogranite of Ferkessédougou. In this study, a total of 281 stream sediment samples and 640 soil samples from the Kangounadéni sector were analyzed to determine the concentrations of 57 major and trace elements, by the multi-acid digestion followed by the ICP-MS multi-element analysis. We processed geochemical analysis results using multivariate statistical techniques including principal component analysis and hierarchical classification, to identify geochemical trends and anomalous zones. Geochemical enrichment in K, Rb, U, and Nb is primarily related to the Ferkessédougou two-micas leucogranite, whereas enrichment in As, Sb, light rare earth elements (LREE), and medium to high contents of Fe, Ni, Cr, and Sc is characteristic of the volcanosedimentary formations. Two types of anomalies have been identified: (i) Li ± Sn anomalies within and around the two-micas Ferkessédougou leucogranite (Li up to 133 ppm in stream sediments and 194 ppm in soils, Sn up to 2.9 ppm in stream sediments and 19.2 ppm in soils), accompanied with high content in Na, K, and Rb in the granite. (ii) Pb-Zn outlying concentrations on its eastern edge, likely associated with meta-volcanosedimentary units (Pb up to 17.24 ppm in stream sediments and 523 ppm in soils, Zn up to 523 ppm in soils). Background thresholds in soils were determined for Li, Pb, Sn, W, Ta, and U at 120

ppm, 109 ppm, 4.1 ppm, 2.3 ppm, 6.6 ppm, and 9.1 ppm, respectively. The Li ± Sn anomalies align with a petrogenetic LCT granite/pegmatite source, related to the two-micas Ferkessédougou leucogranite. However, Nb and Ta concentrations in soils are low, making them unreliable indicators of mineralized zones. Additionally, the Pb-Zn anomaly suggests base metal enrichment linked to a potential sulfide mineralization process within the surrounding volcano-sedimentary rocks. The behavior of HFSE (W, Ti, Nb, Ta) and U is probably controlled by accumulation of residual minerals or laterization.

## Keywords

Banfora, Belt, Exploration, Geochemistry, Anomaly, Mineralization

## 1. Introduction

The West African Craton is made of two shields, namely Reguibat shield in the northern part and Leo/Man shield in the southern part. Both shields comprise a western Archean province with ages between (3500 and 2700 Ma), [1] and an eastern paleoproterozoic province (with ages between 2200 to 2000 Ma), [2] [3]. These two shields are separated by the Neoproterozoic to Phanerozoic Taoudeni basin beneath which are supposed to exist. The Paleoproterozoic domain of the Leo-Man shield, also called the Baoulé-Mossi domain, is made up of greenstone belts and vast gneiss-granitoid domains. The greenstone belts, known as Birimian belt [4]-[6] are made up of ultramafic, mafic, intermediate to felsic volcanosedimentary successions, with geochemical trends evolving from tholeiitic to calc-alkaline signatures. These units also contain detrital sedimentary deposits often identified as late and shallow deposits in the Birimian series [7] [8]. The gneiss-granitoid domains are composed of several generations of amphibole granodiorite/tonalite often assimilated to TTG-type granitoids, biotite granitoids and late alkaline (particularly potassic) granitoids [4] [9]-[14]. These domains also contain foliated and banded granitoids assimilated to migmatites [15] [16] or syntectonic intrusions [17] [18]. The structure of the Baoulé-Mossi domain results from the Eburnean accretional-collisional orogeny, which culminates between Eburnean 2150 and 2100 Ma. This orogeny is manifested by strong crustal growth, by a regional deformation with NE-SW to N-S trend attributed to transpressive deformations and by greenschist-to amphibolite-facies metamorphism [3] [11] [12] [19] [20] (**Figure 1**).

## 2. Geological Context

The Paleoproterozoic Banfora Belt (BB), located in western Burkina Faso, belongs to the Baoulé/Mossi domain of the Léo-Man Shield. It extends over 150 km with an average width of 20 km between the gneiss and granitoid also called Metamorphic and Anatectic Complexes (MAC) of Sidéradougou to the east and Yendéré-Soubakaniédougou to the west [21]. It is covered to the north by the major unconformity

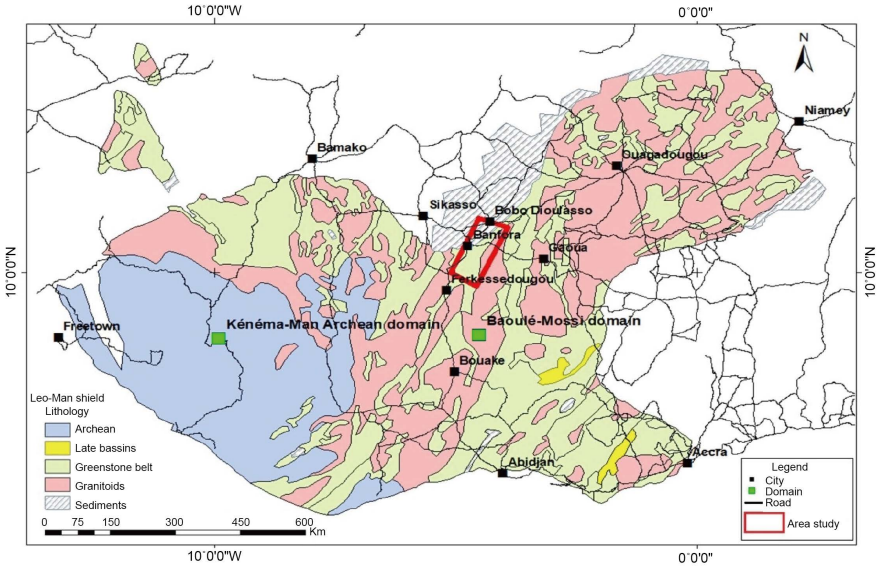


**Figure 1.** Map of the simplified geology of the Man/Leo Shield Modified after [21].

of the Neoproterozoic to Paleozoic sedimentary cover of the Taoudeni basin. It can be structurally split into two corridors of volcanosedimentary units, affected by a metamorphism of greenschist facies. The eastern corridor is composed of intercalations of basalt, pyroxenite, gabbro, andesite, dacite and calc-alkaline rhyolite bordering the MAC of Sidéradougou to the east [21]. This corridor is intruded by the elongated Folonzo biotite and hornblende granite pluton. The Ferkessédougou batholite is composed of a two-micas leucocratic granite (called here two-micas Ferké leucogranite) extended over more than 400 km from Côte d'Ivoire, which crosses the central part of the metasediments on 90 km long, and up to 15 km wide. [22] obtained a U-Pb age of 2094 ± 6 Ma on monazite in the extreme southern part of this batholite in Côte d'Ivoire while [21] obtained a less precise U-Pb age of 2136 ± 40 Ma on zircon in the north-eastern part. Further north, the Dougoulogo elongated quartzo-monzonitic pluton have been dated by [21] at 2182 ± 29 Ma (U-Pb zircon on thin section) (**Figure 2**). An important deformation corridor, the Greenville-Ferkessédougou-Bobo-Dioulasso shear zone (GFBSZ) is made up of a shear zones network that borders the two-micas Ferké leucogranite, then maintains its NNE-SSW orientation in the metasediments until the major unconformity [4]. From a metallogenic point of view, the Baoulé-Mossi domain is a province rich in gold resources [23] [24], but it also has significant potential for other minerals such as base metals [25] and critical metals [26]. In Burkina Faso, prospecting indicators of Pb enrichment are reported at Gan, associated with galena bearing quartz veins [27] and Pb-Zn-bearing sulfides observed in Garango [28] [29]. Elements such as lithium and tin, in demand for their usage in conception of low carbon technologies [30] [31] are attracting, increasing interest in exploration and scientific research. This potential is related in West Africa Craton to the presence of Lithium-Cesium-Tantalite (LCT) pegmatites [32] and mixed LCT + NYF pegmatites [15], related to anatectic melt. Despite

the extensive exploration work carried out on the Banfora belt, for gold and other substances, there is no multi-element geochemical database representative of the geochemical background of the region. Such data cloud has been used as a reference to identify anomalous zones during geochemical explorations, rather than using crustal composition reference values (Clarke), which may not be relevant in metallogenic provinces. As part of the Burkina Faso Mining Sector Development Support Project (PADSEM, funded by World Bank, 2015-2016), geochemical prospecting work in stream sediments in the western and southwestern part of the country was carried out by BUMIGEB. This study highlights the presence of critical metals anomalies (Li, Sn) in the Kangounadéni sector, consistent with the observations of cassiterite and beryl bearing 27, the region's strategic exploration potential in the context of the growing demand for energy transition minerals. In order to constrain these showings and target geochemical anomalies, soil geochemistry work has been carried out in the Kangounadeni sector. In this paper, we present the results of the stream sediment geochemistry and soil geochemistry performed on this study area, and then we identify the ideal chemical indicators for the exploration of the Li ± Sn and Pb-Zn anomalies.

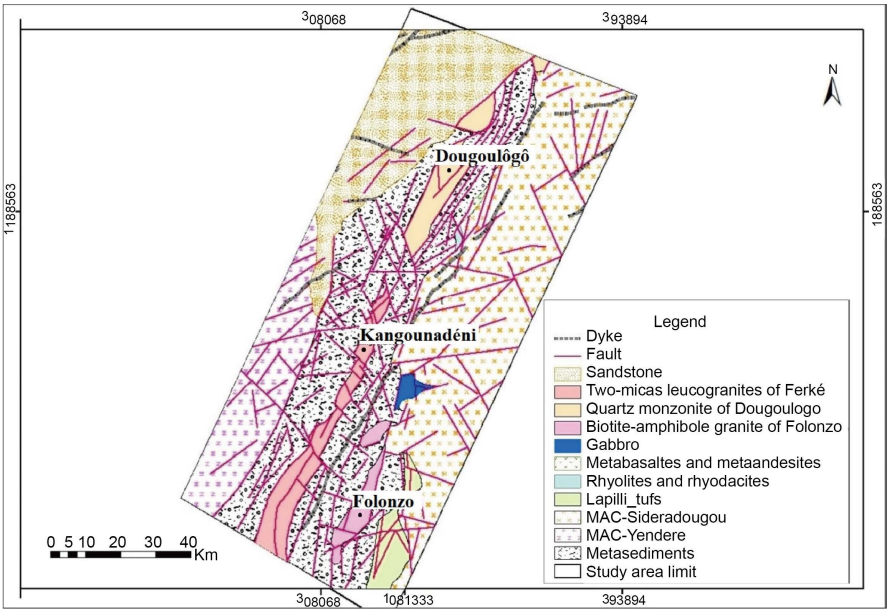


**Figure 2.** Simplified geological map of the studied area (modified after 21).

## 3. Methodology

### 3.1. Sampling Methods

#### 3.1.1. Sampling of Stream Sediments

The stream sediments sampling was carried along a grid which consider one sample per square kilometer (1 sample/km$^2$) between February and March (**Figure 3**). Each sample is a composite of at least 5 sampling points in the fine fraction of sediments in the stream bed, sampled within an interval of several tens meters around the ideal or theoretical sampling point. The average weight of the final

sample is around one kilogram (1 kg). Each sample was taken using a small, tough, non-contaminating plastic scoop.

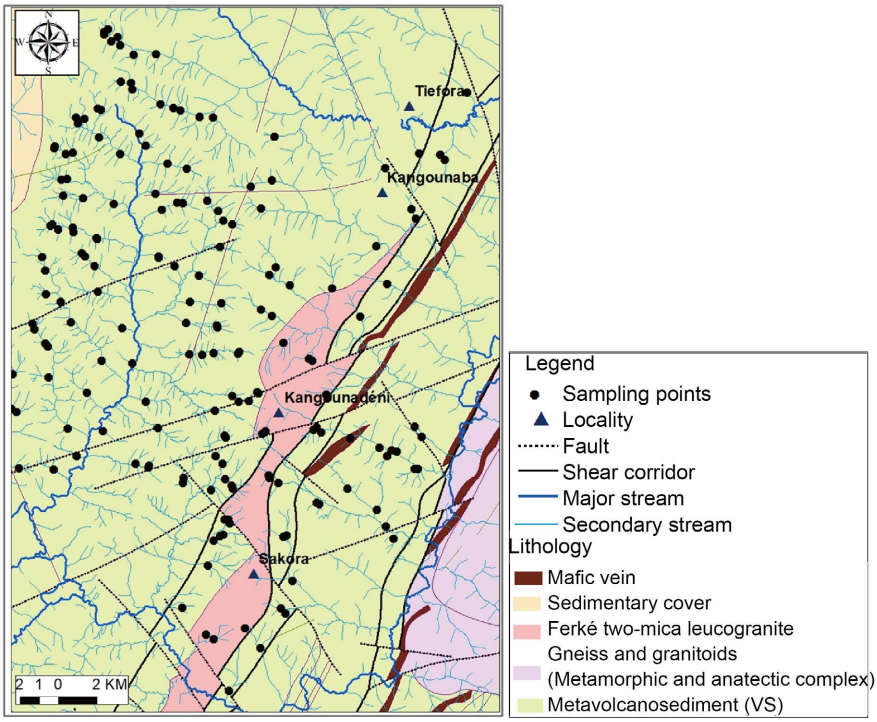


**Figure 3.** Localization of the sampling points on the hydrographic network (21, modified).

### 3.1.2. Soil Sampling

Soil sampling was carried out on a grid of 500 × 200 m over the defined study area, *i.e.* 10 samples per km$^2$ on the anomalies highlighted after the processing and interpretation of the results of the analysis of stream sediments. Depending on the pedo-morpho-regolitic profile encountered, different specific treatments were used for sampling:

**1. Lateritic profile present**

These are the cases where the lateral armour is flush or a gravelly floor covers the breastplate. Under these conditions, the 5 to 10 cm relatively rich in organic matter is stripped with a shovel and the ochre-beige soil rich in sub-centimeter-sized gravel is removed. The biggest fragments (>2 cm) generally quartz is removed manually. If the lateritic crust is flush over a large area, scales of the lateritic crust (chipping with a hammer or crowbar) are taken at least 5 points 10 to 20 m from the central point.

**2. Eroded lateritic profile, saprock or sub-outcropping rock**

This profile is encountered in particular towards the northwest of the prospecting area, whose geology is characterized by sub-outcropping schists, crosscut by quartz veins. At surface, the soil is mainly composed of quartz fragments compared to the shales. The highly altered rock (saprock), clayed, is observed after 3 to 10 cm of stripping. It is this material that is sampled on at least 5 points within a radius of 15 to 20 m around the theoretical point.

**3. Silty plain area and granitic zone**

On lowland areas, it is always difficult to establish whether the cover is real soil or alluvium. In these contexts, the vein is sampled below the humus-bearing horizon at a depth of around 35 cm, taking care to specify on the sampling sheet that it is probably sediment. On the other hand, in certain granitic areas, the sandy horizon encountered at depth (between 30 and 80 cm) is either a granitic arena (*i.e.* saprolite) or transported sandy deposits (*i.e.* sedimentary in nature). The water beneath the slightly organic zone, at a depth of around 15 cm, is sampled and the material (presence of lateritic granules) is carefully described.

## 3.2. Physical Preparation and Analytical Method

### 3.2.1. Analytic Technics for Stream Sediment Samples

The stream sediment samples were spread out in aluminum panels, dried away from sunlight and dust at a temperature not exceeding 40˚C. They were then crushed with porcelain mortar and sieved to 63 µm using a sieve column composed from the bottom to the top, of 63 µm sieve, 125 µm sieve, 150 µm sieve and a lid. The fraction less than 63 µm was quartered by means of a riffle divider so as to obtain 2 sachets of 100 g (+/− 10 g) each.

Samples from the Kangounadéni area were analyzed at the Bureau-Veritas laboratory in Vancouver, Canada using their MA250 method. This multi-acid etching method (hydrochloric, nitric, perchloric and hydrofluoric) is followed by the determination of multi-elements (57 chemical elements) by Inductively Coupled Plasma Mass Spectrometry (ICP-MS).

### 3.2.2. Soil Sample Analysis Methods

The soil samples were spread out in aluminum panels, dried away from sunlight and dust at a temperature not exceeding 40˚C. In order to reduce the particle size, the samples were crushed with porcelain mortar and sieved to 63 µm using a sieve column composed from the bottom to the top, of 63 µm sieve, 125 µm sieve, 150 µm sieve, 2 mm sieve and a lid. The fraction less than 63 µm was quartered by means of a riffle divider so as to obtain 2 sachets of 100 g (+/− 10 g) each. The samples were analyzed at the Bureau-Veritas laboratory in Vancouver, Canada using the MA250 method. The multi-acid etching method (hydrochloric, nitric, perchloric and hydrofluoric) followed by the determination of multi-elements (57 chemical elements) by Inductively Coupled Plasma Mass Spectrometry (ICP-MS).

For all samples, both in stream sediments and in soils, a proportion of 10% of QA/QC samples was integrated to ensure quality control of the analyses. These control samples include blanks, standard and duplicates:

- Blanks: made of white sands from the Bobo-Dioulasso quarry, dried, sieved to 250 µm and then pulverized with an agate bowl. These sands have been used for many years by BUMIGEB as reference blanks for gold analyses.
- Standards: supplied by OREAS (OREAS 45b and OREAS 501c), with certified values for a wide range of chemical elements.
- Duplicates: obtained after sieving, by separation using a riffle separator, to

check the reproducibility of the analyses.

This QA/QC procedure ensures the reliability and accuracy of the geochemical data used for anomaly mapping and subsequent investigations.

# 4. Results

## 4.1. Geochemistry of Stream Sediments

### 4.1.1. Chemical Element Distributions and Anomalous Areas

A total of 281 samples were analyzed and processed. The treatment consisted in the examination of the spatial distribution of the chemical elements; the definition of anomaly thresholds for some key elements (Li, Pb, Sn) and the definition of anomalous areas (Figure 4). The zone located in the continuity of the two-micas

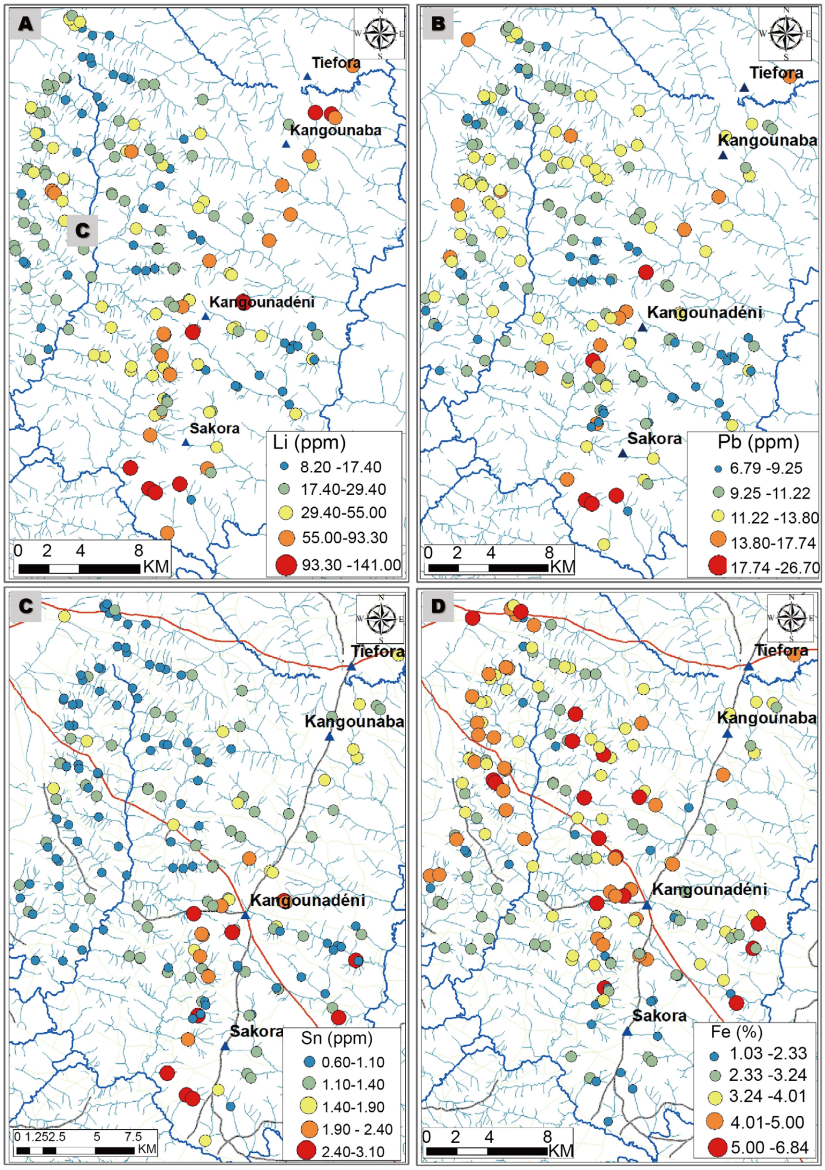


Figure 4. Distribution maps of the elements (A) Li, (B) Pb, (C) Sn and (D) Fe. Lithology refers to the legend in Figure 3.

Ferké leucogranite, presents geochemical disparities compared to the zone located in the western flank (Niarébama-Labola). The axis of the batholith contains the highest concentrations of Li, Be, Cs, Ti, Bi, Nb, Ta, W and Sn (Figure 4 and Figure 5). The extreme northern part of the axis, located in volcanosediments, has samples more enriched in siderophile elements (Fe, Mn, V, Cu, Cr, Mo and Sc), as well as in Cs and Bi. On the other hand, the southern part (Sakora) is richer in K, Rb and U than the northern part. In the northwest, samples from the Niarébama-Labola zone are more enriched in As and Sb compared to those from the batholith axis. As one moves northwest from the central axis of the batholith, there is a gradual enrichment of Zr (Figure 5(A)), Sb, Mo, and REE concentrations (especially marked for light REEs). In contrast, the concentrations of W, Ta and Nb decrease in the same direction (Figure 5(B) and Figure 5(C)).

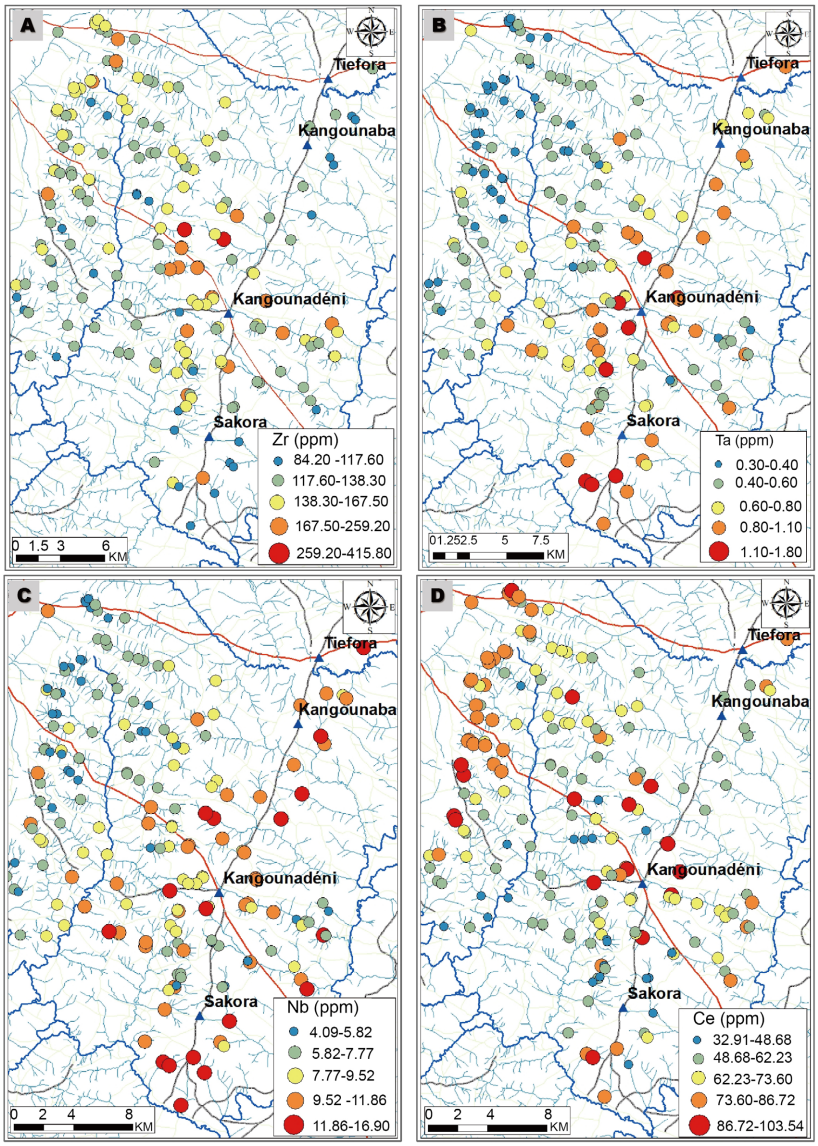


Figure 5. Distribution maps of the elements (A) Zr, (B) Ta, (C) Nb and (D) Ce. Lithology refers to the legend in Figure 3.

#### 4.1.2. Anomalies Detection Thresholds

**1. Lithium (Li)**

As a criterion for discriminating abnormal values in a normal distribution, we use the indicator given by the formula: threshold = mean + 2 * standard deviation [33]. The average concentration of Li in stream sediments is 25.7 ppm (**Figure 6(A)**). This value is significantly higher than the Clarke of Li (21 ppm) [34]. Its geochemical background threshold is calculated at 64.6 ppm. Based on this threshold, five (5) samples are outlying and can be divided into two (2) anomalies, the first is located at the southwest of the village of Sakora (up to 133 ppm). It is located on the two-micas Ferké leucogranite and its orientation is poorly constrained. This area contains points with relatively high concentrations of Rb (up to 226 ppm), U (up to 9.8 ppm), Be (up to 4 ppm), Sn (up to 2.9 ppm) and Ta (up to 1.8 ppm). The second is located at the northeast of the village of Kangounaba. This zone also has points with relatively high concentrations of La (up to 38.7 ppm), Be (up to 5 ppm), Cs (up to 42.9 ppm), and medium concentrations of Sn (up to 1.8 ppm). It is located on the metavolcanosedimentary schists outside the two-micas Ferké leucogranite.

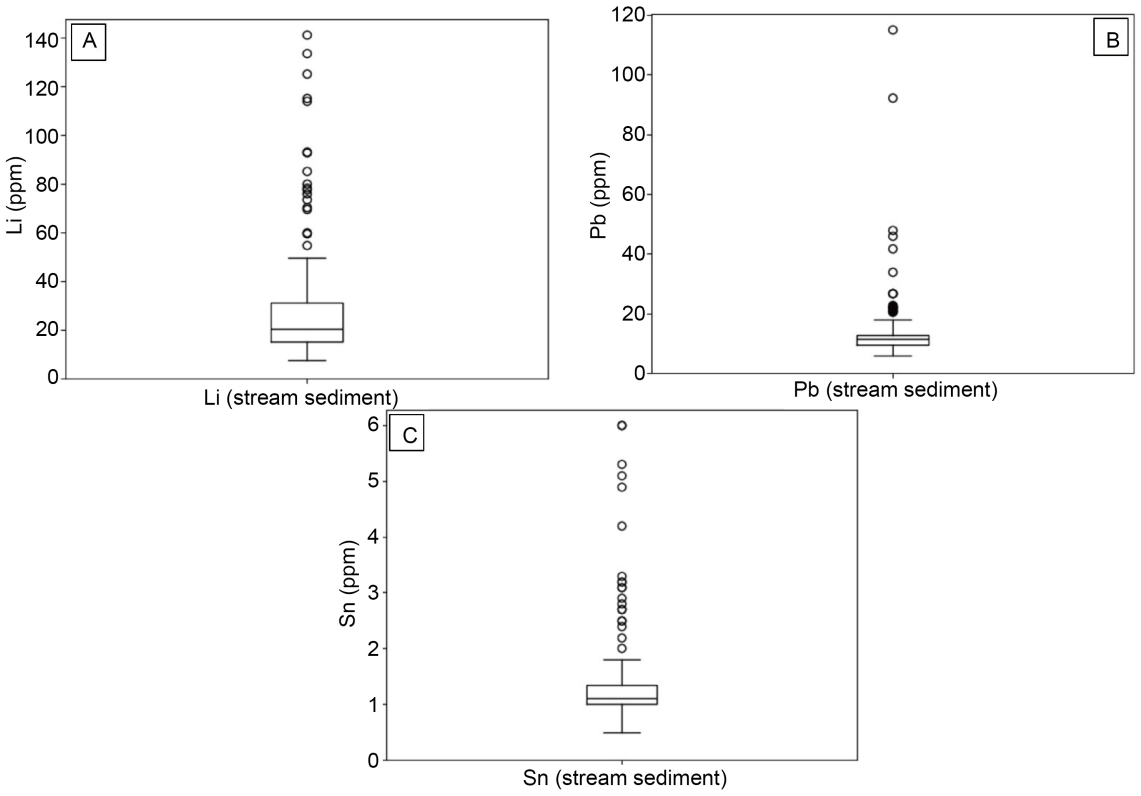


**Figure 6.** (A) Box-plot diagram of the distribution of Li contents; (B) Box-plot diagram of the distribution of Pb contents and (C) Box-plot diagram of the distribution of Sn contents. The box extends from the first quartile to the third quartile. The whiskers extend within 1.5 > the inter-quartile range.

**2. Lead (Pb)**

The average concentration of Pb is 11.60 ppm, which is lower than its Clarke

value (14 ppm) [34] (**Figure 6(B)**). Its geochemical background threshold is calculated at 17.24 ppm. As a result, five (5) sampling points are anomalous: 3 from the south of Sakora (up to 26.7 ppm) on the two-micas Ferké leucogranite and one from the northwestern part of the sampling area (Naniagara-Tangora, up to 17.74 ppm) in the volcanosedimentary shales.

**3. Tin (Sn)**

The average concentration of Sn is 1.2 ppm. This value is much lower than its Clarke (9.8 ppm) [34] (**Figure 6(C)**). Its geochemical background threshold is calculated at 1.93. This results in five (5) points being anomalous, near Sakora, on the leucogranite with two-micas Ferké leucogranite as well as in the surrounding volcanosedimentary units to the west of the village.

### 4.1.3. Anomalies Areas

Regarding to the chemical elements analyzed in the stream sediments, the following anomaly areas were identified (**Figure 7**):

- southwest of the village of Sakora, an anomaly associates the element Li with alkaline elements (K, Rb) as well as with the elements Be, Ta, Sn and U;
- north-east of Kangounaba, an anomaly associates the Li element with the elements Be, Cs, siderophile elements (Fe, Ni, Co) and chalcophile elements (Cr, Mn, Cu, V, Mo, Bi);
- between Naniagara and Tangora: this area contains the highest concentrations of Pb, and especially of As and Sb.

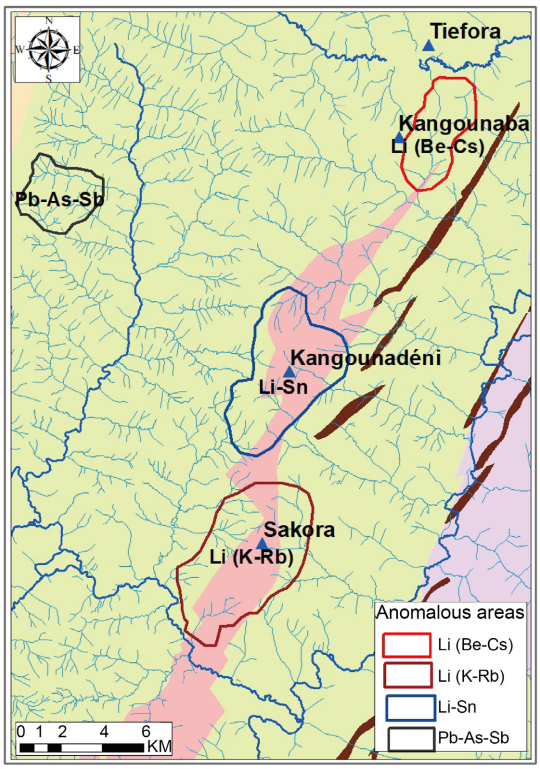


**Figure 7.** Map of anomalous areas of stream sediments on the lithological background in the Kangounadéni sector. Lithology refers to the legend in **Figure 3**.

### 4.2. Soil Geochemistry

A total of 640 samples were chemically analyzed and processed. The treatment was first carried out by describing the spatial distribution of the chemical elements. Then, the identification of abnormal samples, the reduction of variables, principal component analysis and hierarchical ascending classification. At the end of the classification, the dominant chemical behaviours and the areas of anomalies were identified.

#### 4.2.1. Spatial Distribution of Chemical Elements

Analysis of the distribution of chemical elements in soil allows for the identification of general distribution trends. The samples coinciding with the two-micas Ferké leucogranite are relatively richer in alkaline elements (K, Li, Rb), in U and are very depleted in Sc. The K, Li, Rb and Cs elements are particularly enriched along multi-kilometer corridors-oriented NNE-SSW at the south of Sakora and the west of Sakora, ENE-WSW trend at the south of Kangounadéni, but also in less extensive clusters scattered at the north of Kangounadéni. The samples coinciding with the units of the volcanosedimentary belt are relatively more enriched in Sc, W, Cr and Ni.

#### 4.2.2. Anomalous Points

The analysis of the box-plot plots identified a list of samples with very high positive anomalous values in concentrations of Be, Mn, Ba, Ta, W, Pb, Sn and Nb and rare earth elements (Table 1). These samples correspond for the most part to point anomalies, with the exception of two zones at Ta, Be and S, and at Mo and Bi where these anomalies are respectively observed on two neighboring samples.

Table 1. List of samples with extreme values.

| Sample number | Elements and grade | Description | Comment | Anomalous zone identified in this study |
|---|---|---|---|---|
| 456 | Mn (4454 ppm), Ba (909 ppm) | Sample in agricultural land | Point anomaly. Suspected presence of baryte and pyrolusite | Kangounadéni anomaly |
| 473 | Ta (56.1 ppm) | Sample on a lateritic soil | Point anomaly. Suspicion of the presence of Ta-rich refractory minerals | Proximity of the Kangounadéni anomaly |
| 555 | W (6.2 ppm) | Sample in an area of colluvium | Point anomaly in a relatively highly concentrated area to the W | Proximity to the Kangounadéni anomaly |
| 563 | Pb (523.52 ppm) | Highest Pb content, in a lateritic soil 400 m from the road | Point anomaly in NE-SW corridor relatively highly concentrated in Pb | Kangounadéni anomaly |
| 648 | Ta (13.2 ppm) | Sample containing many lateritic granules | Suspicion of the presence of Ta-rich refractory minerals | Proximity of the Kangounadéni anomaly |
| 685 | Eu (2 ppm), Gd (7.4 ppm), Dy (5.2 ppm) | Composite sample on a lateritic area | Outlying REE content | Proximity of the Kangounadéni anomaly |
| 704 | Be (25 ppm) | Sample in agricultural and lateritic soil | Point anomaly | Kangounadéni anomaly |

**Continued**

| | | | | |
|---|---|---|---|---|
| 1001 | Pb (178 ppm) | | Possible anthropogenic contamination, presence of hunting cartridges near the sampling point | South Sakora anomaly (not consistent with Pb concentration) |
| 1021 | Ta (14 ppm) | Sample in a granitic rock environment | Point anomaly, possible presence of Ta-rich refractory minerals. Sample close to Be, Sn cluster | South Sakora anomaly |
| 1023 | Be (34 ppm) | Sample in a granitic rock environment | Cluster restricted to Be, Sn. Typical of LCT-type enrichment | South Sakora anomaly |
| 1024 | Sn (19.2 ppm) | Composite sample in a granitic rock environment | Cluster restricted to Be, Sn. Typical of LCT enrichment | South Sakora anomaly |
| 1105 | Ta (19.9 ppm) | Sample in an agricultural land and laterite environment | Point anomaly. Possible presence of Ta-rich refractory minerals | Proximity of Sakora anomalies |
| 1126 | Mn (5732 ppm), Tl (2.10 ppm) | Sample in a zone of slightly indurated lateritic crust | Point anomaly | Proximity of the Sakora-Nord anomaly |
| 1168 | Nb (29.5 ppm), Ta (37.9 ppm) | Sample on a west-facing slope with abundant laterite granules | Point anomaly. Suspected presence of Ta-rich refractory minerals | Proximity of the Sakora-Nord anomaly |
| 1175 | Mn (7549 ppm), W (6.8 ppm), Ag (1262 ppm), Co (513.9 ppm), Ni (137.7 ppm), Tl (2.64) | Agricultural land with smoky quartz fragments and abundant laterite granules | Point anomaly. Signature of mafic rock | Sakora-North anomaly |
| 1251 | Mo (68.6 ppm) | Sample on a SW slope with quartz and laterite granules | Cluster restricted to Mo, Bi | Kangounaba anomaly |
| 1264 | Bi (138.2 ppm) | Slope to NW with quartz fragments | Cluster restricted to Mo, Bi | Kangounaba anomaly |
| 1265 | Bi (31.29 ppm) | Sample taken in a lateritic environment | Cluster restricted to Mo, Bi | Kangounaba Anomaly |
| 1286 | Pb (289.15 ppm) | Sample taken from a lateritic area with a lot of gravels | Point anomaly in a zone relatively highly concentrated in Pb | Proximity of the Kangounaba anomaly |
| 1295 | Pb (333.21 ppm), W (6,7 ppm) | Sample taken from an environment with quartz and laterite fragments | Point anomaly in a zone relatively highly concentrated in Pb | Proximity to the Kangounaba anomaly |
| 1303 | Ce (439.04 ppm), La (247 ppm), Pr (40.4 ppm), Nd (130.1 ppm), Sm (12.7 ppm), Eu (2.7 ppm), Gd (10.3 ppm) | Sample taken from a lateritic soil with quartz fragments | Anomaly rich in REE | Kangounaba anomaly |

#### 4.2.3. Data Reduction and Principal Component Analysis

**1. Filtering for non-significant and repetitive variables**

For data reduction, our approach is to discard non-significant and repetitive variables. Variables S, Re and Cd were removed because very few samples had concentrations above the detection limits (640, 626, 505, respectively) for a total of 640 analyses. The elements Tm, Lu and Tb have respectively 104, 107 and 186

values above the detection limit. However, they have been removed, but their chemical behaviour can be inferred from the elements Gd and Yb. To identify repetitive variables, we calculated Pearson correlation coefficients that qualify the linear relationship between a pair of variables. Based on a correlation coefficient threshold of 0.75, we grouped the chemical elements into groups, each characterized by a representative element. The variables selected at the end of this treatment are presented in Table 2. Despite the correlations, we have kept some elements because of their geochemical or metallogenic significance. The element Al is kept for the characterization of the aluminosity. The element Th is kept for its metallogenic interest and for the characterization of geochemical mobility compared to U. The elements Cs and Rb are kept despite their correlation with Li and for their use as a marker of enrichment in incompatible elements during magmatic differentiation. Arsenic is kept despite its correlation with Fe, for its metallogenic interest (association with chalcophile elements).

Table 2. Pearson correlation coefficient of soil geochemistry elements.

| Choice of significant variable | Strongly correlated variables (> 0.7) | | | | | | | | Poorly to uncorrelated specific variables | |
|---|---|---|---|---|---|---|---|---|---|---|
| Fe | **V** | **Cr** | **Te** | **In** | **Th** | | | | *Ni* | *Co* |
| | +0.959 | +0.935 | +0.814 | +0.805 | +0.774 | | | | +0.592 | +0.170 |
| Cu | **Ni** | **Sc** | | | | | | | *Zn* | *Pb* |
| | +0.895 | +0.850 | | | | | | | +0.469 | +0.353 |
| La (for light ETRs) | **Ce** | **Pr** | **Nd** | **Sm** | **Eu** | **Gd** | | | | |
| | +0.730 | +0.974 | +0.947 | +0.803 | +0.720 | +0.746 | | | | |
| Gd (for average ETR) | **Pr** | **Nd** | **Sm** | **Eu** | **Tb** | **Dy** | **Ho** | **Er** | | |
| | +0.852 | +0.896 | +0.956 | +0.939 | +0.871 | +0.897 | +0.818 | +0.815 | | |
| Yb (for heavy ETRs) | **Sc** | **Eu** | **Tb** | **Dy** | **Ho** | **Er** | **Tm** | **Lu** | | |
| | 0.830 | 0.836 | 0.815 | +0.927 | +0.933 | +0.965 | +0.850 | +0.840 | | |
| Zr | **Hf** | **Ti** | **Sc** | **Th** | | | | | | |
| | +0.978 | +0.880 | +0.855 | +0.776 | | | | | | |
| As (lessoutliers than Sb) | **Sb** | | | | | | | | | |
| | +0.844 | | | | | | | | | |
| Rb | **K** | **Tl** | **Li** | **Na** | | | | | Cs | |
| | +0.903 | +0.799 | +0.743 | +0.726 | | | | | +0.450 | |
| Al | **Ga** | **In** | **Sc** | **Th** | | | | | | |
| | +0.963 | +0.798 | +0.829 | +0.853 | | | | | | |
| Co (less outliers than Mn) | **Mn** | | | | | | | | | |
| | +0.843 | | | | | | | | | |

After the non-significant and repetitive variables have been excluded, the variables retained for the rest of the analysis are as follows: Li, Be, Na, Mg, Al, P, Ca, Fe, Cu, Co, Zn, As, Se, Rb, Sr, Zr, Nb, Mo, Ag, Sn, Cs, Ba, La, Gd, Yb, Ta, W, Pb, Bi, Th and U. The elements of this selection with a strong correlation (>0.7) are presented in the Table 3.

Table 3. Pearson correlations of chemical elements, above the threshold = 0.7.

| Choice of significant variable | Strongly correlated variables (>0.7) | | | | | | | | Poorly to uncorrelated specific variables | |
|---|---|---|---|---|---|---|---|---|---|---|
| Fe | **V** | **Cr** | **Te** | **In** | **Th** | | | | *Ni* | *Co* |
| | +0.959 | +0.935 | +0.814 | +0.805 | +0.774 | | | | +0.592 | +0.170 |
| Cu | **Ni** | **Sc** | | | | | | | *Zn* | *Pb* |
| | +0.895 | +0.850 | | | | | | | +0.469 | +0.353 |
| La (for light ETRs) | **Ce** | **Pr** | **Nd** | **Sm** | **Eu** | **Gd** | | | | |
| | +0.730 | +0.974 | +0.947 | +0.803 | +0.720 | +0.746 | | | | |
| Gd (for average ETR) | **Pr** | **Nd** | **Sm** | **Eu** | **Tb** | **Dy** | **Ho** | **Er** | | |
| | +0.852 | +0.896 | +0.956 | +0.939 | +0.871 | +0.897 | +0.818 | +0.815 | | |
| Yb (for heavy ETRs) | **Sc** | **Eu** | **Tb** | **Dy** | **Ho** | **Er** | **Tm** | **Lu** | | |
| | 0.830 | 0.836 | 0.815 | +0.927 | +0.933 | +0.965 | +0.850 | +0.840 | | |
| Zr | **Hf** | **Ti** | **Sc** | **Th** | | | | | | |
| | +0.978 | +0.880 | +0.855 | +0.776 | | | | | | |
| As (lessoutliers than Sb) | **Sb** | | | | | | | | | |
| | +0.844 | | | | | | | | | |
| Rb | **K** | **Tl** | **Li** | **Na** | | | | | Cs | |
| | +0.903 | +0.799 | +0.743 | +0.726 | | | | | +0.450 | |
| Al | **Ga** | **In** | **Sc** | **Th** | | | | | | |
| | +0.963 | +0.798 | +0.829 | +0.853 | | | | | | |
| Co (less outliers than Mn) | **Mn** | | | | | | | | | |
| | +0.843 | | | | | | | | | |

### 2. Principal component analysis

A principal component analysis (PCA) was carried out on the 31 elements retained with all 640 samples. The first three factors express a cumulative variance of 53.11% (Table 4).

Table 4. Eigenvalues of the first 3 factors.

| | F1 | F2 | F3 |
|---|---|---|---|
| Eigenvalue | 8.102 | 5.304 | 3.085 |
| Variability (%) | 26.093 | 17.082 | 9.936 |
| % cumulative | 26.093 | 43.175 | 53.111 |

Factor 1 shows an opposition between a positive pole dominated by Th, immobile elements (Al, Fe, Zr) and heavy REE, and an alkaline negative pole represented by the elements Li, Na and Rb (Table 5). The F2 factor opposes a positive pole dominated by alkaline earth elements (Mg, Ca, Sr, Ba), and a negative pole dominated by organophile elements (P, As, Se, U), and siderophile. In the factor diagram, the distribution of chemical elements indicates an opposition between alkaline and alkaline earth elements associated with Li (negative F1 and positive F2), and organophile and semimetal elements (positive F1 and negative F2). The F3 factor is controlled by the elements Sn, U, P, Li in opposition to certain incompatible elements of high load (medium and heavy REE, Zr, W), and elements with calcium tendency (Ba, Mg, Ca) and chalcophile (Co, Cu, Zn) (Table 5). The Ta element does not have a noticeable influence in the three (3) main factors, which is characterized by its scores close to zero in them (Figure 8).

Table 5. Summary of the first three factors.

| Factor | Negative pole | Positive pole |
|---|---|---|
| F1 | Rb, Na, Li | Th, Fe, Al, Zr, Cu, Yb, W |
| F2 | As, Fe, Se, U, P, Th | Sr, Ba, Li, Mg, Cs, Ca |
| F3 | Yb, Mg, Co, Ba, Cu, W, Gd, Zn, Zr, Ca | U, Sn, P, Be, Li |

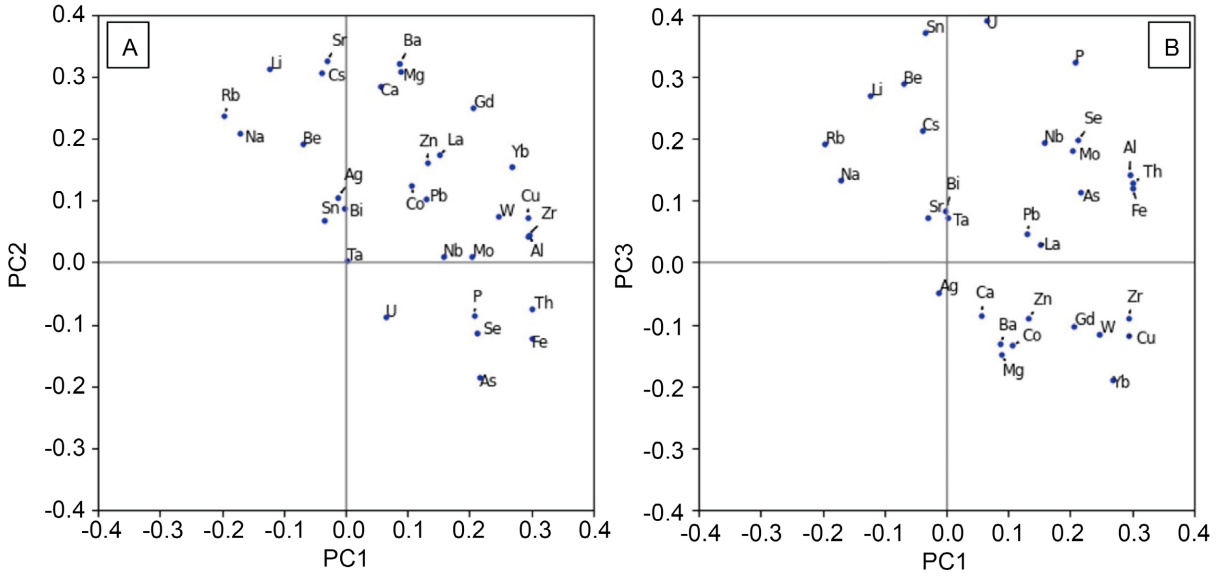


Figure 8. Factor diagrams of the components: (A) F1 vs F2 and (B) F1 vs F3.

### 4.2.4. Hierarchical Ascending Classification

We performed a hierarchical ascending classification using all the analysis results, transformed into a centered log-ratio for the same elements selected for the principal component analysis. Agglomerative hierarchical clustering was applied using Ward's linkage with Euclidean distance. The clustering quality indices gave a low silhouette score (0.158) and a moderate cophenetic correlation (0.573) indi-

cating weak separation between groups. However, the choice of five (5) classes is justified by the observed consistency between the clusters (Table 6), the identified anomalies, and the lithologies of the sampling areas (Table 7). The dendrogram is shown in Figure 9. Classes C1 and C5 coincide spatially with volcanosediments. They also contain the samples with the highest Cu values ($\mu$ = 56 ppm). Class C5 is characterized by high values in Mg but also in Li ($\mu$ = 60 ppm) and is exclusively observed in the North. Classes C2, C3 and C4 coincide with two-micas Ferké leucogranite. Class C3 particularly the two previous ones by relatively high concentrations of U ($\mu$ = 6 ppm). The other two classes C2 and C4 have relatively low values of Fe, Al, As and Th. The class C2 corresponds to the zone of Li anomaly ($\mu$ = 69 ppm) and contains samples rich in Na and K, but depleted in REE. These two trends allow us to group these classes into two (2) superclasses, the CVS class (C1 + C5) which contains the analyses with a volcanosedimentary type signature and the CGR class (C2 + C3 + C4) which contains the granitic type signatures. Li-rich samples are preferentially found in classes C2 and C5, each corresponding respectively to the anomalous class in Li in its superclass CGR and CVS (Figure 10).

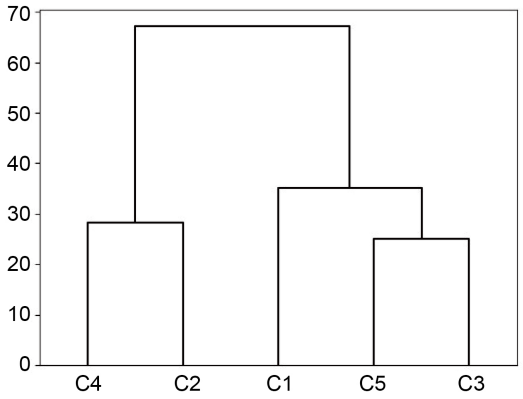


Figure 9. Classification tree after hierarchical clustering of filtered sample soils composition.

Table 6. Average values of hierarchical classes from soil geochemistry. Maximum values are in bold.

| | C1 | C2 | C3 | C4 | C5 |
|---|---|---|---|---|---|
| Mo | 3.31 | 0.64 | 3.71 | 0.83 | **8.85** |
| Pb | 41.11 | 23.11 | 31.23 | 21.77 | **63.20** |
| Zn | **48.06** | 20.43 | 22.83 | 29.26 | 34.17 |
| Fe | **13.31** | 2.23 | 10.76 | 3.17 | 12.47 |
| U | 3.26 | 3.52 | **6.44** | 2.62 | 2.61 |
| Sr | 18.60 | 38.59 | 20.51 | 27.87 | **42.46** |
| Bi | 0.34 | 1.14 | 0.95 | 0.60 | **6.15** |
| Ca | 0.03 | 0.03 | 0.03 | 0.05 | **0.05** |
| P | 0.03 | 0.02 | **0.04** | 0.01 | 0.04 |

**Continued**

| | | | | | |
|---|---|---|---|---|---|
| Mg | 0.09 | 0.06 | 0.06 | 0.13 | **0.15** |
| Ba | 198.42 | 182.00 | 124.45 | 191.26 | **253.11** |
| Al | **6.13** | 3.54 | 5.50 | 4.24 | 6.02 |
| Na | 0.04 | **0.30** | 0.03 | 0.10 | 0.05 |
| W | 1.33 | 0.40 | 0.68 | 0.75 | **1.60** |
| Sn | 1.43 | **2.24** | 2.10 | 1.76 | 1.34 |
| Yb | 0.92 | 0.34 | 0.63 | 0.76 | **1.17** |
| Li | 17.55 | **68.57** | 32.06 | 44.12 | 59.91 |
| Ta | 0.56 | 0.87 | **1.67** | 0.73 | 0.49 |
| Nb | 6.93 | 5.48 | **8.07** | 7.19 | 6.57 |
| Cs | 3.06 | 11.88 | 5.63 | 7.92 | **24.02** |
| Cu | 46.39 | 7.20 | 25.27 | 19.84 | **56.76** |
| Ag | 64.77 | 70.22 | 42.35 | **71.28** | 56.11 |
| Be | 1.46 | 3.97 | 2.45 | 1.92 | **4.00** |
| Se | 0.41 | 0.21 | **0.43** | 0.21 | 0.39 |
| Co | 16.15 | 2.22 | 6.44 | 8.04 | **20.45** |
| As | **18.16** | 3.06 | 12.42 | 3.13 | 6.49 |
| Th | **6.88** | 2.76 | 6.48 | 4.03 | 6.33 |
| La | 15.23 | 9.03 | 14.79 | 13.89 | **35.36** |
| Gd | 2.02 | 1.15 | 1.64 | 1.95 | **3.03** |
| Rb | 40.67 | **124.59** | 48.36 | 70.32 | 46.92 |
| Zr | **85.24** | 46.48 | 70.30 | 72.77 | 80.96 |

**Table 7.** Lithogeochemical interpretation of the different classes.

| Classe | Enrichment | Depletion | Interpretation |
|---|---|---|---|
| C1 | Fe, Cr, Sc, Cu | Li | Volcanosediments |
| C2 | Li, Na, K, Rb | Fe, Al, Cu, Cr, ETR Lourdes, Te, Ni, As, Th, Ti, Sc, Hf, Zr, V | Granite + alkaline enrichment + Li enrichment |
| C3 | Fe, U, Sb, Cr | Ba, Li | Granite + lateritization (+Fe, Al) |
| C4 | | Fe, P, Cr, Te, As, Th, V | Granite |
| C5 | Li, Fe, Cr, Mg, Sc, Cu | | Volcanosediments + Li enrichment |

#### 4.2.5. Anomalies Thresholds

**1. Lithium (Li)**

As a criterion for discriminating abnormal values in a normal distribution, we use the indicator given by the formula: threshold = mean + 2 * standard deviation [33]. The concentration of Li in soil samples averages 37 ppm, which is higher than the Clarke of Li (20 ppm) [34]. In the CVS superclass, this average is 25 ppm, while it is 47 ppm in the CGR superclass (**Figure 11**). The granitic batholith is

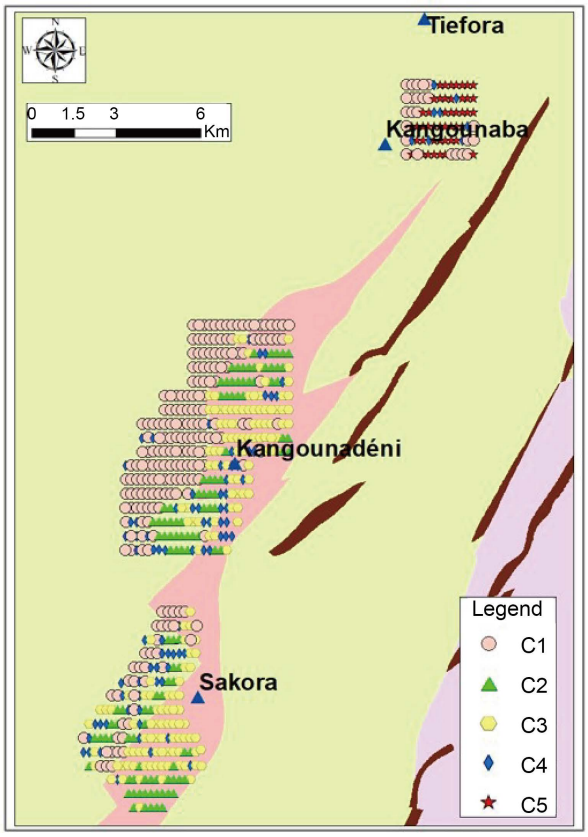


**Figure 10.** Hierarchical classes of samples on lithological map background. Lithology refers to the legend in **Figure 3**.

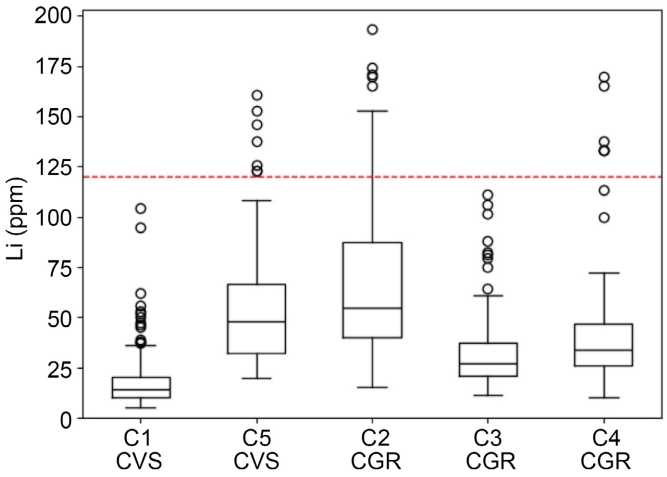


**Figure 11.** Box-plot diagram of the distribution of Li contents. Boxplot defined as in **Figure 5**.

therefore naturally richer in Li than the volcanosedimentary host. The geochemical background threshold of Li for the dataset is 120 ppm. About 4.5% of the samples have values above this threshold. These samples are located south of Tiéfora (Kougounaba, up to 170 ppm), south of Kangounadéni (up to 175 ppm) and south of Sakora (up to 194 ppm). The area at the southernmost point of the Kangoun-

adéni anomaly has a Li ± Sn signature with some high Sn grades at 6.4 ppm.

Thus, four anomalies are highlighted in the study area (Figure 12):

- The Kangounaba anomaly is trending NNE-SSW, 3 kilometers long and nearly 1.5 km wide. This anomaly coincides with point anomalies in Mo and Bi, and relatively high concentrations in Cs.
- The Kangounadéni anomaly is oriented NNE-SSW, on the western edge of the two-micas Ferké leucogranite. It is 9 km long, with a width of 1 km in the north to 2 km in the south.
- Two anomalies are identifiable around Sakora. To the north-east of the village, an anomalous zone oriented NEE-SSW extends over 4 km long and 1 km wide. To the south of the village, an ENE-SWS oriented anomaly extends over 4 km long and 1.5 km wide.

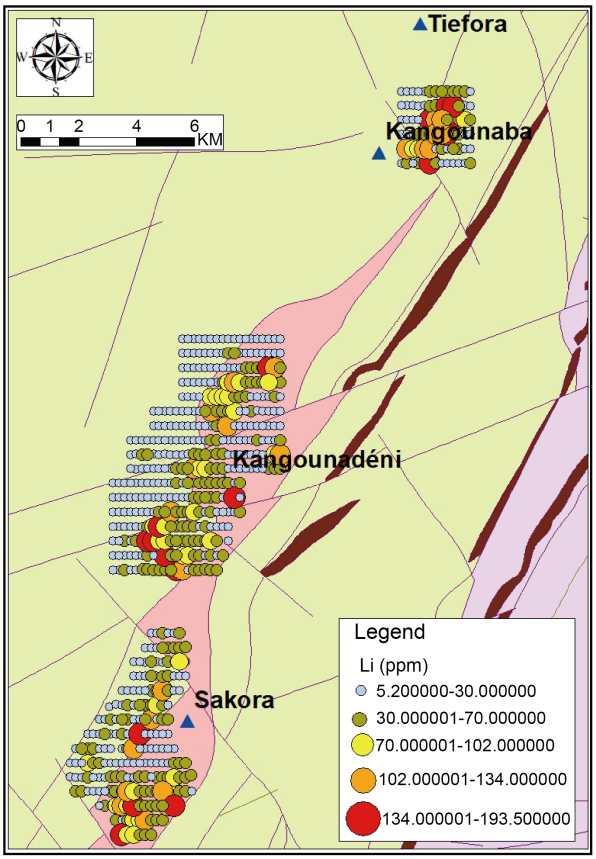


Figure 12. Map of Li soil anomalies on the lithological background in the Kangounadéni sector. Lithology refers to the legend in Figure 3.

### 2. Lead-Zinc (Pb-Zn)

The average concentration of Pb (Figure 13(A)) is 34 ppm, which is much higher than Clarke (14 ppm) [34]. In addition, nearly 82% of the analyses are superior to the Clarke. The calculated geochemical background threshold is 109 ppm, which leaves 25 samples (approximately 4%) in anomalous concentration. These samples are found exclusively west of Kangounaba, and in Kangounadéni.

The average concentration of Zn (Figure 13(B)) is 33 ppm. This average is much lower than the Clarke of Zn which is (70 - 80 ppm) [34]. The calculated geochemical background is 93 ppm, which leaves 25 samples (about 4%) in anomalous concentrations. With the exception of a point anomaly observed near Sakora, anomalous points with respect to the threshold are located at Kangounadéni (up to 523 ppm). We have retained as an anomalous zone a corridor-oriented NNE-SSW, west of Kangounadéni, which coincides with the edge of the batholith. This corridor is 8 km long, and its widest area is 1.8 km (Figure 14).

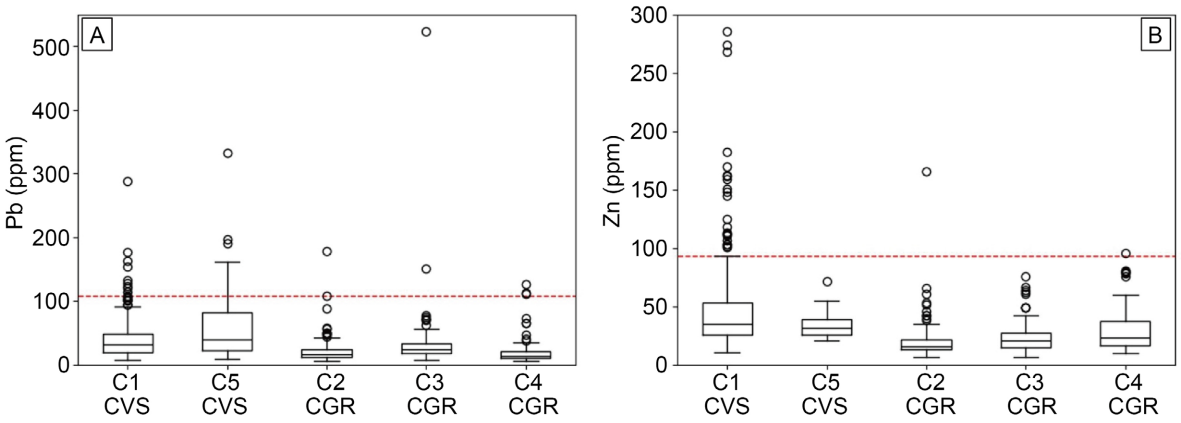


Figure 13. (A) Box-plots of Pb and (B) Zn concentrations in soil samples. Boxplots defined as in Figure 5.

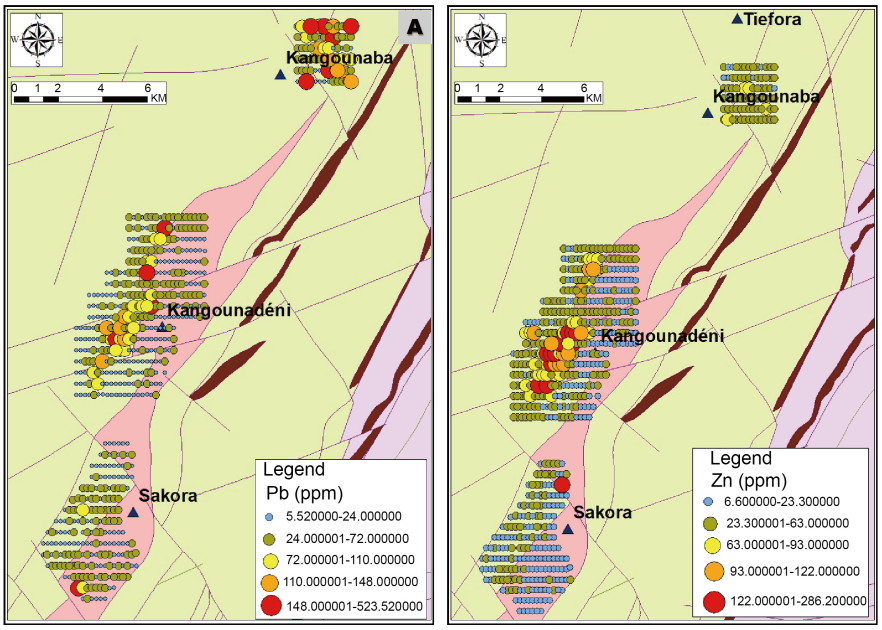


Figure 14. Map of (A) Pb and (B) Zn soil anomalies on a lithological background in the Kangounadéni sector. Lithology refers to the legend in Figure 3.

### 3. Rare Earth Elements (La-Ce-Nd)

The element La (Figure 15(A)) has an average in soil samples of 15 ppm, which is lower than Clarke (39 ppm) [34]. The geochemical background threshold (42

ppm) is close to the Clarke, leaving only 9 anomalous samples rich in La. These two samples are located exclusively in the anomalous Li-zone at Kangounaba (up to 247 ppm). The element Ce (**Figure 15(B)**) has an average in soil samples of 39 ppm, lower than its Clarke (66.5 ppm) [34]. On the other hand, its geochemical background threshold is high (109 ppm), which leaves less than 5% anomalous samples. These samples are all distributed in Li-anomalous zones with concentrations especially high in the Kangounaba anomaly (up to 439 ppm). The element Nd (**Figure 15(C)**) has an average in soil samples of 12 ppm, which is lower than its Clarke (41.5 ppm) (Lide, 2005). Its geochemical background threshold is calculated at 28 ppm, which leaves less than 3% anomalous samples. These samples are located on the Kangounaba (up to 162 ppm) and Kangounadéni (up to 66 ppm) Li anomalies. The element Dy has an average in soil samples of 1.37 ppm, which is lower than its Clarke (5.2 ppm) (Lide, 2005). Its geochemical background threshold is calculated at 2.59 ppm, which remains lower than the Clarke and leaves less than 4.6% anomalous samples. These samples are located in the Li anomalous zones of Kangounaba and Kangounadéni. Ultimately, the REE anomaly zones coincide with those of the Li in the Kangounaba (volcanosedimentary zone) and Kangounadéni (granitic zone) parts.

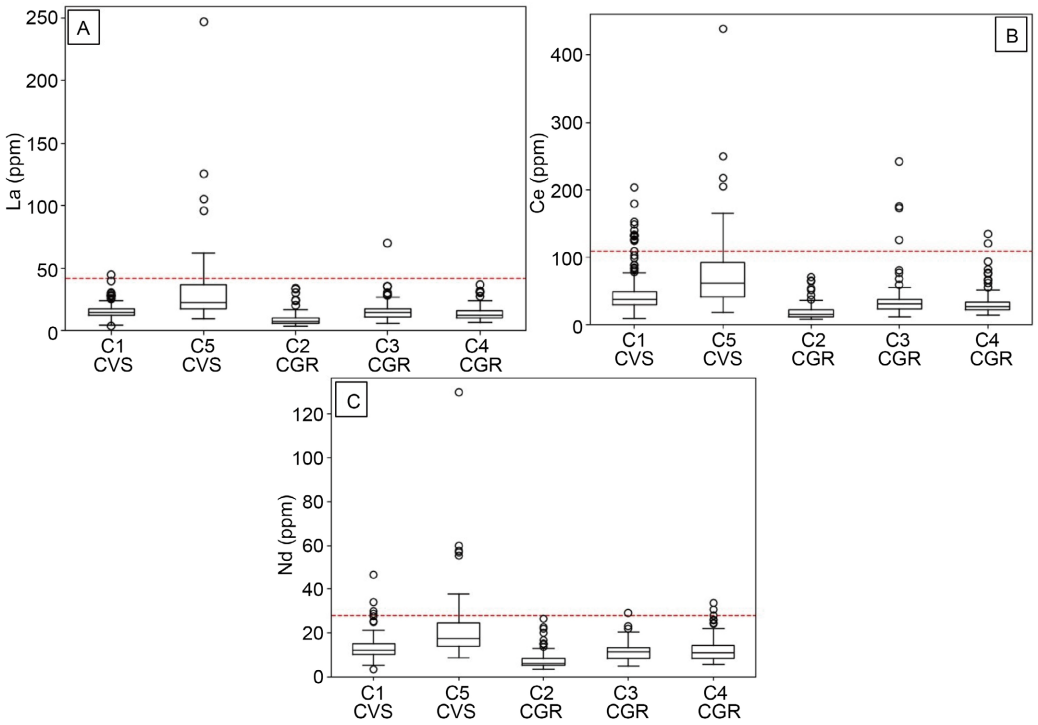


**Figure 15.** Box-plots of (A) La, (B) Ce contents and (C) Nd concentrations in soil samples. Boxplots defined as in **Figure 5**.

### 4. Sn, W, Ta and U anomalies

Tin has an average content of 1.8 ppm in soil samples, lower than its Clarke (9.8 ppm). Its geochemical background threshold is calculated at 4.1 ppm, which

leaves less than 2.7% of anomalous samples, which are located in the Li-anomalous zones of Kangounadéni (up to 8 ppm) and Sakora (up to 19.2 ppm). Tungsten has an average content of 0.9 ppm in soil samples, lower than its Clarke (1.25). Its geochemical background threshold is calculated at 2.3 ppm, which leaves about 2% of anomalous samples that are located in the Li-anomalous zones of Kangounadéni (up to 6.2 ppm) and Kangounaba (up to 6.7 ppm). A point anomaly is also observed North of Sakora (6.8 ppm). Tantalum has an average content of 0.9 ppm in soil samples, lower than its Clarke (2.0 ppm). Its geochemical background threshold is calculated at 6.6 ppm, which leaves only 6 anomalous samples. These samples are scattered around the Kangounadéni (up to 56 ppm) and Sakora (up to 37 ppm) Li anomalies. Uranium has an average content of 4.0 ppm in soil samples, higher than its Clarke (2.7 ppm). Its geochemical background threshold is set at 9.1 ppm, which leaves 5.5% anomalous samples (35 samples). These samples are located in the anomalous zones of Kangounadéni (up to 18.2 ppm) and Sakora (up to 14.5 ppm).

### 4.3. Assessment of Anomalous Areas Based on Stream Sediment and Soil Data

The anomalous zones of Kangounaba and Sakora observed in stream sediments are also found in soils. However, the enrichments observed in each type of rock may show slight variations. The sampling density allowed the Sakora level to distinguish two sub-enrichment zones, one to the north of the locality, and the other to the south (Figure 16). The F1 component of the PCA shows the trend in

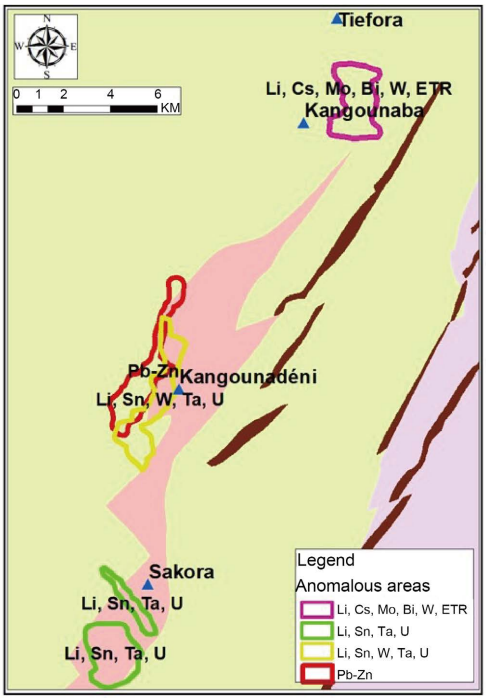


Figure 16. Map of anomalies in the study area. Lithology refers to the legend in Figure 3.

Li-Rb enrichment (F1 < 0). However, this alone is not sufficient to constrain the anomaly observed at Kangounaba. The Pb-Zn anomalies observed east of Kangounadéni correspond to samples of class C1, identified as representing volcanosedimentary units. This association suggests that the anomaly is hosted in volcanosedimentary units, and not in the two-micas Ferké leucogranite (Table 8).

Table 8. Summary of anomalous areas.

| | | Stream sediment | | | Soils | | |
|---|---|---|---|---|---|---|---|
| Dominant-related lithology | Geochemical signature sub-family | General Distribution | Anomalies Identified | Trends + anomalies | PCA | Hierarchical classification | Anomalies identified |
| Volcanosediment | Volcanosediment signature-NW | More enriched in As, Sb, light REE. Medium to high values of Fe, Mn, Ni, Co, Cr, Cu, V | | Higher in Ni, Cr, Sc and W | −3 < F1 < 6 | CVS-C1 (Fe, Cr, Sc, Cu) | |
| | Naniagara-Tangora | | Pb | | | | Not sampled |
| | NE volcanosediment: Kangounaba anomaly | Enriched in Li, Be, Cs, Ti, Bi, Nb, Ta, W, Sn and U | High values of Li, as well as Be, Cs, Mo, Bi, light REE. | Point anomalies in Mo, Bi, Pb | −3 < F1 < 6 | CVS-C5 (Li, Fe, Cr, Mg, Sc, Cu) | Li, Cs, Mo, Bi, W, ETR |
| Two-micas Ferké leucogranite | Signature type of granitoids | More enriched in Li, Be, Cs, Ti, Bi, Nb, Ta, W, Sn and U<br>Lower in V | | Richer in Li, K, Rb, U, Nb than samples from volcanosedimentary contexts | | CGR-C3, C4 | |
| | Kangounadéni anomaly (Pb-Zn) | Not sampled | Not sampled | Point anomalies in Ta, W, Pb, ETR | | CVS-C1 | Pb-Zn |
| | Kangounadéni anomaly (Li) | Not sampled | Not sampled | | | | Li, Sn, W, Ta, U |
| | Sakora Nord anomaly | | | Point anomalies in Mn, Tl, Nb, Ta, Ni, Co, Ag, W | F1 < 0 | CGR-C2 (Li, Na, K, Rb) | Li, Sn, Ta, U |
| | Sakora Sud anomaly | | High values for Li, as well as Be, Rb, Sn, Ta and U | Point anomalies in Be, Sn, Ta | | | Li, Sn, Ta, U |

## 5. Discussion

### 5.1. Chemical Dispersion of W, Nb, Ta and U

In stream sediments, a decrease in the concentration of the elements W, Nb and Ta is observed from the edge of the batholith to the northeast. These elements are among high field strength elements (HFSEs), usually behaving as immobile elements during meteoric weathering [35] [36]. They are likely to be reconcentrated on the surface on the one hand by the relative accumulation during meteoric weathering, and on the other hand by the trapping of oxides carrying these ele-

ments. In addition, the refractory minerals zircon, rutile and columbo-tantalite could be carriers of Nb and Ta in sediments [37]. The observed Pearson correlations between the elements W and Ti (0.609), Nb and Ti (0.804), and Ta and Ti (0.697) suggest that the presence of titanium oxide primarily controls W, Nb, and Ta concentrations. In soils, W tungsten is depleted from granitic zones to volcanosedimentary zones, but the elements Nb and Ta do not show a consistent distribution with lithology. The distribution of uranium U in soils is due to several different processes. The highest concentrations of U are observed in soil samples around Kangounadéni and Sakora (19 samples at U > 11 ppm). They are higher than the average concentrations found worldwide in soils [38]. Specifically, the most extreme values are found near Kangounadéni, on covers corresponding to the lateritic surfaces of high glacis. It is therefore very likely that the concentration of U in soils is partly linked to supergene accumulation (preferably in clays) during episodes of lateritic cover formation. The element U is found to be very weakly correlated with P (Pearson coefficient = 0.549), Sb (Pearson coefficient = 0.509), V (Pearson coefficient = 0.461) and Sn (Pearson coefficient = 0.407). On the one hand, the association with the organophile elements P and Sb suggests that the U concentration is controlled by organic matter. On the other hand, it is also associated with soils of hierarchical class C3, which corresponds to less evolved granitic units (low concentration of Ba, Li) and high concentration of Fe compared to the other granitic classes. This distribution is not consistent with the natural tendency of uranium enrichment with differentiation in peraluminous magmas [39], and rather suggests a depletion of the U during the magmatic differentiation of the two-micas Ferké leucogranite, coupled with a fractionation induced by meteoric oxidation.

### 5.2. Cu-Mo/Bi/Pb-Zn Concentration Indicator

In the Kangounaba area, high concentrations of Cu, Mo and Bi are observed in soil samples. Although these concentrations are found sporadically, they may reflect geochemical trends of Cu-Mo association in the form of a "nugget effect" due to the presence of bearing minerals (molybdenite, or secondary oxides and clays) that have maintained or enhanced these concentrations. The Cu-Mo association is usually observed in deposits in a magmatic-hydrothermal transition context, e.g. skarns and porphyries [40]-[42], while Bi can also be associated with Cu-Pb or Pb-Zn sulfide mineralization resulting from hydrothermal episodes [43]. The abundance of Mo in pegmatites is mentioned in the literature, but is generally associated with Sn-W mineralization (cassiterite, wolframite) [44] [45]. Since Cu, Mo are Bi are not associated with Li enrichment in the Kangounaba area, the hypothesis of an enrichment related to magmatic evolution of the two-micas Ferké leucogranite can be ruled out. In view of the difference in the geochemical trend of Cu-Mo-Bi enrichment between the Kangounaba anomaly and the Kangounadéni-Sakora anomalies, we can assume the existence of a not unearthed intrusion or a distant intrusion), whose exsolution of late-magmatic fluids is at the origin of

hydrothermal alteration in the Kangounaba zone.

The Dougoulogo massif in the North, has significant Cu concentrations (10 - 50 ppm) but lacks Bi and Mo, (Bi < 1 ppm, Mo below the detection limit) [46], reflecting remobilization from deep source. Cu is concentrated in the oxidized horizons by hydrothermal or meteoric transport, while Bi and Mo, less mobile, remain at depth, explaining their low concentration at the surface [47].

A pole of Pb-Zn enrichment is clearly identifiable to the west of Kangounadéni, and seems to correspond to a kilometric lens at the edge of the two-micas Ferké leucogranite, enriched in Zn (up to 286 ppm), Pb (up to 523 ppm), Ag (up to 182 ppm) and depleted in Bi (<1 ppm). This type of association is typical of polymetallic sulfide deposits, generally associated with the circulation of hydrothermal fluids of metamorphic origin such as Sedimentary Exhalative Deposit (SEDEX) and the formation of sulphide associated mineralization [48]. As the geological context of the Banfora belt does not exhibit evidence of a paleo unconformity (birimian sedimentary of a pre/early birimian basement), it is more likely that the anomalies observed derive from a context similar to that of the VMS, which are also observed in other Birimian belts of the Baoulé-Mossi domain [49]-[51].

### 5.3. Li Concentration Indicators Lithium-Cesium-Tantalum (LCT) Type

The Li-Sn geochemical anomalies are commonly observed in rare metal granite/pegmatite deposits of the Lithium-Cesium-Tantalum (LCT) petrogenetic family [52] [53]. These pegmatites are generally associated with peraluminous granites, and are most of the time interpreted as resulting from fractional crystallization, resulting in a concentration of alkaline elements (Li, K, Rb, ...), and fluxing elements (B, F, P, ...) and $H_2O$ [54]-[56]. These processes are accompanied by a more or less notable enrichment in Nb, Ta and Sn. The geological setting of the Banfora belt presents an ideal configuration to host this type of mineralization. Indeed, the two-micas Ferké leucogranite is a peraluminous granite and therefore a potential parent source for Li-Rb enrichments. Its geochemistry exhibits stronger REE depletion, compared to calc-alkaline plutonic rocks of the BB (Dougoulogo and Folonzo granite), with Li concentration up to 320 ppm, but low content in Sn (<6 ppm) and Cs (<44 ppm) [46]. In general, peraluminous granites tend to deplete Zr and REE during differentiation [57]. This feature is observed in soil geochemistry samples, which are depleted in Zr and REE in granitic zones compared to volcanosediments, suggesting that the underlying granite is depleted of REE. The granitic zone specifically exhibits an enrichment in Li, Be, Cs, Nb, Ta, W and Sn in stream sediment geochemistry and Li, K, Rb, U and Nb in soils geochemistry, consistent with granitic fractionated signature with increasing content in Nb, Ta, W and Sn. Then, the Li ± Sn soils anomalies are located in the northeastern margin of the batholith, which according to an inverse zonation model with differentiated leucogranitic margins [58] could derive from localized late magmatic facies or from late pegmatite dikes intrusive in volcanosediments. A

similar setting is observed in the batholith of Kédougou-Kéniéba inliner, where spodumene-bearing pegmatites, dikes are described in the extreme northeastern part of the granitic batholith of Saraya [59]. According to the typical zonation model of LCT pegmatites around their source pluton [60], the proximal pegmatites are enriched in Be, then Nb and Ta, while the distal pegmatites show the most pronounced enrichments in Li, Cs and Ta. This setting is not perceptible in our context, where the Li and Be elements are enriched in both the granitic massif and the surrounding area, while the Sn and Rb elements seem to be mainly concentrated in the anomalies within the batholith (especially in the granitic corridors defined from class C2). The highest Cs content (with also Ca and Mg) is specifically found in the north out of the granitic body, suggesting a geochemical enrichment trend different from the Li-Rb-trend in granitic facies, and controlled by alkaline earth elements. As in the case of the Saraya batholith, this model is not suitable for the elongated structure of the batholith, because the zones of Li enrichment correspond more to lateral margin of a granite massif rather than the roof of the intrusion. The samples classified C2 (granitic trend, Li-rich) are distributed in the form of clusters often extended over 2 to 3 km in NE-SW, N-S and NW-SE orientations in the Kangounadéni zone, and NESW in the Sakora zone. These oriented clusters suggest the presence of linear anomalies that could be attributed to enriched pegmatite veins. Apart from this, the C2 point clusters are distributed on the hillsides of a ridge line extending from Kangounadéni to Sakora, around high lateritic glacis, [61]. The areas corresponding to the glacis are covered mainly by C3 points. This is consistent with the observed association of C3 points with enrichment in Fe, Al, and suggests that in these areas, Li and Ba concentrations are depleted by lateralization (**Table 7**).

### 5.4. Limits to the Use of Soil Geochemistry and Stream Geochemistry

Apart from samples of very anomalous values in Ta concentration (mainly class C3 and of class C2, <19 ppm < Ta < 57 ppm), Ta concentrations are generally homogeneous throughout the surveyed area, with a slight depletion in the extreme northern part. Niobium also follows this same trend, with many more anomalous points. Although these Ta concentrations are significantly high for soil samples (overall average at 1 ppm, [36], principal component analysis shows that Ta does not contribute significantly to the data set. It therefore does not follow any of the geochemical trends identified for the elements (alkaline, alkaline-earth, organophile or siderophile elements). Moreover, the highest values in Ta and Nb do not coincide with the enrichments observed in Li. As suggested above, the high concentrations of Ta could result from the accumulation of Fe/Ti oxides, and this tendency of gravitational accumulation is therefore not perceptible through the multi-criteria analysis of the data. Either the potential for Nb/Ta enrichment of the identified anomalies is low to the detriment of Sn, or these elements constitute poor indicators for the search for differentiated and enriched zones in our study

area. In addition, interpretation biases can be induced by the choice of variables for the analysis of anomalies. The Li anomaly observed in the Kangounaba zone coincides with high values in Fe, Co, Cu, Mu, which we attribute to a signature deriving from the host volcanosedimentary units. However, the component analysis shows an opposition between the alkaline chemical elements (Li, K, Rb) and the siderophile elements, particularly according to the B component. An interpretation based solely on the principal component analysis could lead to the elimination of units rich in siderophile elements, whereas in our context Li enrichment is superimposed on rocks rich in siderophile elements. In addition, the principal component analysis highlights more the overall geochemical affinities of the lithologies rather than the enrichment trends of the targeted elements (Li, Nb, Ta, ...).

## 6. Conclusion

The results of geochemical prospecting of stream sediments and soil geochemistry revealed anomalous associations of Li ± K ± Rb ± Sn in the two-micas Ferké leucogranite, Li ± Be ± Cs in surrounding rocks in the north of the two-micas Ferké leucogranite, and Pb-Zn in a delimited west margin of the leucogranite. The geochemical anomalies identified in stream sediments were confirmed by soil geochemistry that better highlights the opposed behavior of Li vs REE (opposed for example in F1 in PCA), or the association of Li with Sn, Ta and U inside the leucogranite, but does not exhibit an enrichment of Be with Li. The Li-Sn anomalies are consistent with a geochemical signature of LCT (lithium-cesium-tantalum) granites/pegmatites, but Nb and Ta concentrations are low in soils samples, making them unreliable indicators of a mineralized zone. Through hierarchical classification, two geochemical backgrounds were identified: one associated with volcanic-sedimentary rocks characterized by higher content in Fe, Cr, Sc and Cu, and the other associated with the two-micas Ferké leucogranite and characterized by higher alkaline content (K, Na, Rb), and REE depletion. The granitic background can be affected by lateritization, resulting in a decrease of Li and Ba content, and an increase of Fe and Al. These backgrounds control the overall geochemical signature and can lead to misinterpretations if the focus is exclusively on elemental concentration.

## Acknowledgements

This work has benefited from the material and financial support of the Bureau of Mines and Geology of Burkina Faso (BUMIGEB), National Geological Survey.

## Conflicts of Interest

The authors declare no conflicts of interest regarding the publication of this paper.

## References

[1] Rollinson, H. (2016) Archaean Crustal Evolution in West Africa: A New Synthesis of

the Archaean Geology in Sierra Leone, Liberia, Guinea and Ivory Coast. *Precambrian Research*, **281**, 1-12.

[2] Parra-Avila, L.A., Baratoux, L., Eglinger, A., Fiorentini, M.L. and Block, S. (2019) The Eburnean Magmatic Evolution across the Baoulé-Mossi Domain: Geodynamic Implications for the West African Craton. *Precambrian Research*, **332**, Article ID: 105392. https://doi.org/10.1016/j.precamres.2019.105392

[3] Grenholm, M., Jessell, M. and Thébaud, N. (2019) A Geodynamic Model for the Paleoproterozoic (Ca. 2.27 - 1.96 Ga) Birimian Orogen of the Southern West African Craton—Insights into an Evolving Accretionary-Collisional Orogenic System. *Earth-Science Reviews*, **192**, 138-193. https://doi.org/10.1016/j.earscirev.2019.02.006

[4] Baratoux, L., Metelka, V., Naba, S., Jessell, M.W., Grégoire, M. and Ganne, J. (2011) Juvenile Paleoproterozoic Crust Evolution during the Eburnean Orogeny (~2.2 - 2.0 Ga), Western Burkina Faso. *Precambrian Research*, **191**, 18-45. https://doi.org/10.1016/j.precamres.2011.08.010

[5] Labou, I., Benoit, M., Baratoux, L., Grégoire, M., Ndiaye, P.M., Thebaud, N., *et al.* (2020) Petrological and Geochemical Study of Birimian Ultramafic Rocks within the West African Craton: Insights from Mako (Senegal) and Loraboué (Burkina Faso) Lherzolite/Harzburgite/Wehrlite Associations. *Journal of African Earth Sciences*, **162**, Article ID: 103677. https://doi.org/10.1016/j.jafrearsci.2019.103677

[6] Mériaud, N., Thébaud, N., Masurel, Q., Hayman, P., Jessell, M., Kemp, A., *et al.* (2020) Lithostratigraphic Evolution of the Bandamian Volcanic Cycle in Central Côte d'Ivoire: Insights into the Late Eburnean Magmatic Resurgence and Its Geodynamic Implications. *Precambrian Research*, **347**, Article ID: 105847. https://doi.org/10.1016/j.precamres.2020.105847

[7] Pigois, J., Groves, D.I., Fletcher, I.R., McNaughton, N.J. and Snee, L.W. (2003) Age Constraints on Tarkwaian Palaeoplacer and Lode-Gold Formation in the Tarkwa-Damang District, SW Ghana. *Mineralium Deposita*, **38**, 695-714. https://doi.org/10.1007/s00126-003-0360-5

[8] Koffi, Y.H., Wenmenga, U. and Djro, S.C. (2016) Tarkwaian Deposits of the Birimian Belt of Houndé: Petrological, Structural and Geochemical Study (Burkina-Faso, West Africa). *International Journal of Geosciences*, **7**, 685-700. https://doi.org/10.4236/ijg.2016.75053

[9] Castaing, C., Billa, M., Milési, J., Thiéblemont, D., Le Metour, J., Egal, E., *et al.* (2003) Notice explicative de la Carte géologique et minière du Burkina Faso à 1/1,000,000. Bureau de Recherches Géologiques et Minières (BRGM)/Bureau des Mines et de la Géologie du Burkina (BUMIGEB).

[10] Naba, S., Lompo, M., Debat, P., Bouchez, J.L. and Béziat, D. (2004) Structure and Emplacement Model for Late-Orogenic Paleoproterozoic Granitoids: The Tenkodogo-Yamba Elongate Pluton (Eastern Burkina Faso). *Journal of African Earth Sciences*, **38**, 41-57. https://doi.org/10.1016/j.jafrearsci.2003.09.004

[11] Lompo, M. (2009) Geodynamic Evolution of the 2.25 - 2.0 Ga Palaeoproterozoic Magmatic Rocks in the Man-Leo Shield of the West African Craton. A Model of Subsidence of an Oceanic Plateau. *Geological Society, London, Special Publications*, **323**, 231-254. https://doi.org/10.1144/sp323.11

[12] Vidal, M., Gumiaux, C., Cagnard, F., Pouclet, A., Ouattara, G. and Pichon, M. (2009) Evolution of a Paleoproterozoic "Weak Type" Orogeny in the West African Craton (Ivory Coast). *Tectonophysics*, **477**, 145-159. https://doi.org/10.1016/j.tecto.2009.02.010

[13] Lambert-Smith, J.S., Lawrence, D.M., Müller, W. and Treloar, P.J. (2016) Palaeotec-

tonic Setting of the South-Eastern Kédougou-Kéniéba Inlier, West Africa: New Insights from Igneous Trace Element Geochemistry and U-Pb Zircon Ages. *Precambrian Research*, **274**, 110-135. https://doi.org/10.1016/j.precamres.2015.10.013

[14] Sakyi, P.A., Addae, R.A., Su, B., Dampare, S.B., Abitty, E., Su, B., *et al.* (2020) Petrology and Geochemistry of TTG and K-Rich Paleoproterozoic Birimian Granitoids of the West African Craton (Ghana): Petrogenesis and Tectonic Implications. *Precambrian Research*, **336**, Article ID: 105492. https://doi.org/10.1016/j.precamres.2019.105492

[15] Bonzi, W.M., Van Lichtervelde, M., Vanderhaeghe, O., André-Mayer, A., Salvi, S. and Wenmenga, U. (2022) Insights from Mineral Trace Chemistry on the Origin of NYF and Mixed LCT + NYF Pegmatites and Their Mineralization at Mangodara, SW Burkina Faso. *Mineralium Deposita*, **58**, 75-104. https://doi.org/10.1007/s00126-022-01127-x

[16] Bonzi, W.M., Vanderhaeghe, O., Van Lichtervelde, M., Wenmenga, U., André-Mayer, A., Salvi, S., *et al.* (2021) Petrogenetic Links between Rare Metal-Bearing Pegmatites and TTG Gneisses in the West African Craton: The Mangodara District of SW Burkina Faso. *Precambrian Research*, **364**, Article ID: 106359. https://doi.org/10.1016/j.precamres.2021.106359

[17] Hirdes, W. and Davis, D.W. (2002) U-Pb Geochronology of Paleoproterozoic Rocks in the Southern Part of the Kedougou-Kéniéba Inlier, Senegal, West Africa: Evidence for Diachronous Accretionary Development of the Eburnean Province. *Precambrian Research*, **118**, 83-99. https://doi.org/10.1016/s0301-9268(02)00080-3

[18] Lahondère, D., Thiéblemont, D., Tegyey, M., Guerrot, C. and Diabate, B. (2002) First Evidence of Early Birimian (2.21 Ga) Volcanic Activity in Upper Guinea: The Volcanics and Associated Rocks of the Niani Suite. *Journal of African Earth Sciences*, **35**, 417-431. https://doi.org/10.1016/s0899-5362(02)00145-8

[19] Ganne, J., De Andrade, V., Weinberg, R.F., Vidal, O., Dubacq, B., Kagambega, N., *et al.* (2011) Modern-Style Plate Subduction Preserved in the Palaeoproterozoic West African Craton. *Nature Geoscience*, **5**, 60-65. https://doi.org/10.1038/ngeo1321

[20] Parra-Avila, L.A., Kemp, A.I.S., Fiorentini, M.L., Belousova, E., Baratoux, L., Block, S., *et al.* (2017) The Geochronological Evolution of the Paleoproterozoic Baoulé-Mossi Domain of the Southern West African Craton. *Precambrian Research*, **300**, 1-27. https://doi.org/10.1016/j.precamres.2017.07.036

[21] Giovenazzo, D., Ouedraogo, C., Séjourné, S., Hein, K.A.A., Jébrak, M., Malo, M., *et al.* (2018) Notice explicative de la carte géologique 1/200,000, Feuille NC-30-XIV, Banfora-Kong, Ef-figis Géo-Solutions.

[22] Doumbia, S., Pouclet, A., Kouamelan, A., Peucat, J.J., Vidal, M. and Delor, C. (1998) Petrogenesis of Juvenile-Type Birimian (Paleoproterozoic) Granitoids in Central Côte-d'Ivoire, West Africa: Geochemistry and Geochronology. *Precambrian Research*, **87**, 33-63. https://doi.org/10.1016/s0301-9268(97)00201-5

[23] Goldfarb, R.J., André-Mayer, A., Jowitt, S.M. and Mudd, G.M. (2017) West Africa: The World's Premier Paleoproterozoic Gold Province. *Economic Geology*, **112**, 123-143. https://doi.org/10.2113/econgeo.112.1.123

[24] Masurel, Q., Eglinger, A., Thébaud, N., Allibone, A., André-Mayer, A., McFarlane, H., *et al.* (2021) Paleoproterozoic Gold Events in the Southern West African Craton: Review and Synopsis. *Mineralium Deposita*, **57**, 513-537. https://doi.org/10.1007/s00126-021-01052-5

[25] Markwitz, V., Hein, K.A.A., Jessell, M.W. and Miller, J. (2016) Metallogenic Portfolio of the West Africa Craton. *Ore Geology Reviews*, **78**, 558-563.

https://doi.org/10.1016/j.oregeorev.2015.10.024

[26] Kazapoe, R.W. (2023) Assessing the Lithium Potential of the Paleoproterozoic Rocks of the West African Craton; the Case So Far. *Geosystem Engineering*, **26**, 257-271. https://doi.org/10.1080/12269328.2023.2229351

[27] Hottin, G. and Ouédraogo, O.F. (1975) Carte geologique de la Republique de Haute-volta 1:1,000,000 [Geological Map of the Republic of Haute-Volta 1: 1,000,000.] Rép. de Haute-Volta. Ministère du commerce, du développement industriel et des mines, Direction de la géologie et des mines, Ouagadougou.

[28] Langerien, C. (1975) Recherche du Pb-Zn dans les séries différenciées calco-magnésiennes du socle libérien. Rapp. B.R.G.M., 23.

[29] Autran, A. (1975) Résultat obtenu en 1975 sur le permis de Tenkodogo (secteur de Ouenzeogo). 125, Rapp. B.R.G.M., 3.

[30] Harper, E.M., Kavlak, G., Burmeister, L., Eckelman, M.J., Erbis, S., Sebastian Espinoza, V., *et al.* (2015) Criticality of the Geological Zinc, Tin, and Lead Family. *Journal of Industrial Ecology*, **19**, 628-644. https://doi.org/10.1111/jiec.12213

[31] Tabelin, C.B., Dallas, J., Casanova, S., Pelech, T., Bournival, G., Saydam, S., *et al.* (2021) Towards a Low-Carbon Society: A Review of Lithium Resource Availability, Challenges and Innovations in Mining, Extraction and Recycling, and Future Perspectives. *Minerals Engineering*, **163**, Article ID: 106743. https://doi.org/10.1016/j.mineng.2020.106743

[32] Adams, S.J., Van Lichtervelde, M., Amponsah, P.O., Nude, P.M., Asiedu, D.K. and Dampare, S.B. (2023) Characterisation and Rare-Metal Potential of the Winneba-Mankoadze Pegmatites, Southern Ghana: Evidence of Two Pegmatite Fields. *Journal of African Earth Sciences*, **207**, Article ID: 105049. https://doi.org/10.1016/j.jafrearsci.2023.105049

[33] Erhardt, W., Höpker, K.A. and Fischer, I. (1996) Bewertungsverfahren Verfahren zur Bewertung von immissionsbedingten Stoffanreicherungen in standardisierten Graskulturen. *Umweltwissenschaften und Schadstoff-Forschung*, **8**, 237-240. https://doi.org/10.1007/bf02940467

[34] Lide, D.R. (2005) Abundance of Elements in the Earth's Crust and in the Sea. In: Rumble, J., Ed., *CRC Handbook of Chemistry and Physics*, CRC Press, 14-17.

[35] Scheib, A.J., Flight, D.M.A., Birke, M., Tarvainen, T. and Locutura, J. (2012) The Geochemistry of Niobium and Its Distribution and Relative Mobility in Agricultural Soils of Europe. *Geochemistry*: *Exploration*, *Environment*, *Analysis*, **12**, 293-302. https://doi.org/10.1144/geochem2011-096

[36] Filella, M. (2017) Tantalum in the Environment. *Earth-Science Reviews*, **173**, 122-140. https://doi.org/10.1016/j.earscirev.2017.07.002

[37] Dill, H.G., Melcher, F., Füßl, M. and Weber, B. (2006) Accessory Minerals in Cassiterite: A Tool for Provenance and Environmental Analyses of Colluvial-Fluvial Placer Deposits (NE Bavaria, Germany). *Sedimentary Geology*, **191**, 171-189. https://doi.org/10.1016/j.sedgeo.2006.03.022

[38] Kabata-Pendias, A. (2000) Trace Elements in Soils and Plants. 3rd Edition, CRC Press.

[39] Cuney, M. (2014) Felsic Magmatism and Uranium Deposits. *Bulletin de la Société Géologique de France*, **185**, 75-92. https://doi.org/10.2113/gssgfbull.185.2.75

[40] Zhou, H., Sun, X., Fu, Y., Lin, H. and Jiang, L. (2016) Mineralogy and Mineral Chemistry of Bi-Minerals: Constraints on Ore Genesis of the Beiya Giant Porphyry-Skarn Gold Deposit, Southwestern China. *Ore Geology Reviews*, **79**, 408-424.

https://doi.org/10.1016/j.oregeorev.2016.06.008

[41] Kovalenker, V.A., Trubkin, N.V., Abramova, V.D., Plotinskaya, O.Y., Kiseleva, G.D., Borisovskii, S.E., *et al.* (2018) Typomorphic Characteristics of Molybdenite from the Bystrinsky Cu-Au Porphyry-Skarn Deposit, Eastern Transbaikal Region, Russia. *Geology of Ore Deposits*, **60**, 62-81. https://doi.org/10.1134/s107570151801004x

[42] Fu, Y., Peng, Z., Wang, B., Wang, G., Hu, J., Guan, J., *et al.* (2021) Petrology and Metamorphism of Glaucophane Eclogites in Changning-Menglian Suture Zone, Bangbing Area, Southeast Tibetan Plateau: A Evidence for Paleo-Tethyan Subduction. *China Geology*, **4**, 1-16. https://doi.org/10.31035/cg2021017

[43] Pažout, R., Sejkora, J. and Šrein, V. (2017) Bismuth and Bismuth-Antimony Sulphosalts from Kutná Hora Vein Ag-Pb-Zn Ore District, Czech Republic. *Journal of Geosciences*, **62**, 59-76. https://doi.org/10.3190/jgeosci.230

[44] Kontak, D.J., Creaser, R.A., Heaman, L.M. and Archibald, D.A. (2005) U-Pb Tantalite, Re-Os Molybdenite, and 40Ar/39Ar Muscovite Dating of the Brazil Lake Pegmatite, Nova Scotia: A Possible Shear-Zone Related Origin for an LCT-Type Pegmatite. *Atlantic Geology*, **41**, 17-29. https://doi.org/10.4138/655

[45] Stein, H.J. (2006) Low-Rhenium Molybdenite by Metamorphism in Northern Sweden: Recognition, Genesis, and Global Implications. *Lithos*, **87**, 300-327. https://doi.org/10.1016/j.lithos.2005.06.014

[46] Ouedraogo, A., Naba, S. and Ilboudo, H. (2024) Petrographic and Geochemical Characters of Granites of the Banfora Belt, Burkina Faso (West Africa). *International Journal of Geosciences*, **15**, 682-697. https://doi.org/10.4236/ijg.2024.159038

[47] Chavez, W.X. (2021) Weathering of Copper Deposits and Copper Mobility: Mineralogy, Geochemical Stratigraphy, and Exploration Implications. *SEG Discovery*, **126**, 16-27. https://doi.org/10.5382/SEGnews.2021-126.fea-01

[48] Sangster, D.F. (2017) Toward an Integrated Genetic Model for Vent-Distal SEDEX Deposits. *Mineralium Deposita*, **53**, 509-527. https://doi.org/10.1007/s00126-017-0755-3

[49] Ilboudo, H., Lompo, M., Wenmenga, U., Napon, S., Naba, S. and Ngom, P.M. (2017) Evidence of a Volcanogenic Massive Sulfide (Zn Pb Cu Ag) District within the Tiébélé Birimian (Paleoproterozoic) Greenstone Belts, Southern Burkina Faso (West-Africa). *Journal of African Earth Sciences*, **129**, 792-813. https://doi.org/10.1016/j.jafrearsci.2017.01.020

[50] Ilboudo, H., Sawadogo, S., Kagambega, N. and Remmal, T. (2021) Petrology, Geochemistry, and Source of the Emplacement Model of the Paleoproterozoic Tiébélé Granite Pluton, Burkina Faso (West-Africa): Contribution to Mineral Exploration. *International Journal of Earth Sciences*, **110**, 1753-1781. https://doi.org/10.1007/s00531-021-02039-3

[51] Schwartz, M.O. and Melcher, F. (2003) The Perkoa Zinc Deposit, Burkina Faso. *Economic Geology*, **98**, 1463-1485. https://doi.org/10.2113/gsecongeo.98.7.1463

[52] Černý, P., Blevin, P.L., Cuney, M. and London, D. (2005) Granite-Related Ore Deposits. *Society of Economic Geologists*, **100**, 337-370.

[53] London, D. (2005) Granitic Pegmatites: An Assessment of Current Concepts and Directions for the Future. *Lithos*, **80**, 281-303. https://doi.org/10.1016/j.lithos.2004.02.009

[54] London, D. (2018) Ore-Forming Processes within Granitic Pegmatites. *Ore Geology Reviews*, **101**, 349-383. https://doi.org/10.1016/j.oregeorev.2018.04.020

[55] Nabelek, P.I., Whittington, A.G. and Sirbescu, M.C. (2009) The Role of $H_2O$ in Rapid

Emplacement and Crystallization of Granite Pegmatites: Resolving the Paradox of Large Crystals in Highly Undercooled Melts. *Contributions to Mineralogy and Petrology*, **160**, 313-325. https://doi.org/10.1007/s00410-009-0479-1

[56] Thomas, R. and Davidson, P. (2016) Revisiting Complete Miscibility between Silicate Melts and Hydrous Fluids, and the Extreme Enrichment of Some Elements in the Supercritical State—Consequences for the Formation of Pegmatites and Ore Deposits. *Ore Geology Reviews*, **72**, 1088-1101. https://doi.org/10.1016/j.oregeorev.2015.10.004

[57] Linnen, R.L. and Cuney, M. (2005) Granite-Related Rare-Element Deposits and Experimental Constraints on Ta-Nb-W-Sn-Zr-Hf Mineralization. In: Linnen, R.L. and Samson, I.M., Eds., *Rare-Element Geochemistry and Mineral Deposits* (*Vol.* 17), Geological Association of Canada Short Course Notes, 45-68.

[58] Trubač, J., Janoušek, V., Žák, J., Somr, M., Kabele, P., Švancara, J., *et al.* (2017) Origin of Reverse Compositional and Textural Zoning in Granite Plutons by Localized Thermal Overturn of Stratified Magma Chambers. *Lithos*, **277**, 315-336. https://doi.org/10.1016/j.lithos.2016.10.002

[59] Delor, C., Couëffé, R., Goujou, J., Diallo, D., Théveniaut, H., Fullgraf, T., Ndiaye, P., Dioh, E., Blein, O. and Barry, T. (2010) Notice explicative de la carte géologique à 1/200,000 du Sénégal, feuille Saraya-Kédougou Est. Ministère des Mines, de l'Industrie, de l'Agro-Industrie et des PME, Direction des Mines et de la Géologie, Dakar.

[60] Hulsbosch, N., Boiron, M., Thomas, R., Van Daele, J., Dewaele, S. and Muchez, P. (2019) Evaluation of the Petrogenetic Significance of Melt Inclusions in Pegmatitic Schorl-Dravite from Graphic Tourmaline-Quartz Assemblages: Application of LA-ICP-QMS Analyses and Volume Ratio Calculations. *Geochimica et Cosmochimica Acta*, **244**, 308-335. https://doi.org/10.1016/j.gca.2018.10.023

[61] Grimaud, J., Chardon, D., Metelka, V., Beauvais, A. and Bamba, O. (2015) Neogene Cratonic Erosion Fluxes and Landform Evolution Processes from Regional Regolith Mapping (Burkina Faso, West Africa). *Geomorphology*, **241**, 315-330. https://doi.org/10.1016/j.geomorph.2015.04.006